Carbonate clumped isotope bond reordering and geospeedometry

Benjamin H. Passey *, Gregory A. Henkes

Department of Earth and Planetary Sciences, Johns Hopkins University, 3400 N Charles Street, Baltimore, MD 21218, USA

ABSTRACT

Carbonate clumped isotope thermometry is based on the preference of ^{13}C and ^{18}O to form bonds with each other. At elevated temperatures such bond ordering is susceptible to resetting by diffusion of C and O through the solid mineral lattice. This type of bond reordering has the potential to obscure primary paleoclimate information, but could also provide a basis for reconstructing shallow crustal temperatures and cooling rates. We determined Arrhenius parameters for solid-state reordering of C–O bonds in two different calcites through a series of laboratory heating experiments. We find that the calcites have different susceptibilities to solid-state reordering. Reaction progress follows a first order rate law in both calcites, but only after an initial period of non-first order reaction that we suggest relates to annealing of nonequilibrium defects when the calcites are first heated to experimental temperature. We show that the apparent equilibrium temperature equations (or "closure temperature" equations) for carbonate clumped isotope reordering are analogous to Dodson's equations for first order loss of daughter isotopes. For each calcite, the sensitivity of apparent equilibrium temperature to cooling rate is sufficiently high for inference of cooling rates within a factor of ~ 5 or better for cooling rates ranging from tens of degrees per day to a few degrees per million years. However, because the calcites have different susceptibilities to reordering, each calcite defines its own cooling rate–apparent equilibrium temperature relationship.

The cooling rates of Carrara marble inferred from carbonate clumped isotope geospeedometry are 10^{-6}–10^{-3} degrees per annum and are in broad agreement with rates inferred from thermochronometric methods. Cooling rates for ^{13}C-depleted calcites from the late Neoproterozoic Doushantou cap carbonates in south China are on the order of 10^{2}–10^{4} degrees per annum, consistent with rapid cooling following formation of these calcites by a short-lived hydrothermal event (Bristow et al., 2011, Nature v. 474, p. 68–71). Most of the uncertainty in these estimates relates to uncertainty in Arrhenius parameters for different calcites. Thus, while the carbonate clumped isotope geospeedometer shows promise for recording cooling rates in settings and lithologies where other geospeedometers may not be applicable, the uncertainty in cooling rate will be large without independent knowledge of the reordering kinetics of each study material. Thus the full potential of the method will only be realized if reordering kinetics can be accurately determined for each study material, or predicted on the basis of mineral composition, texture, or other observable parameters.

1. Introduction

The carbonate clumped isotope thermometer (Ghosh et al., 2006; Schauble et al., 2006) is based on the temperature dependence of homogeneous order/disorder reactions, specifically for calcium carbonate,

$$Ca^{13}C^{16}O_3 + Ca^{12}C^{18}O^{16}O_2 \leftrightarrow Ca^{13}C^{18}O^{16}O_2 + Ca^{12}C^{16}O_3 \qquad (1)$$
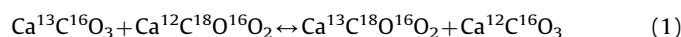
While many applications of this thermometer have related to paleoclimate (e.g., Came et al., 2007; Finnegan et al., 2011; Keating-Bitonti et al., 2011), the thermometer promises to be useful as a geothermometer in the ~ 50–$300\ ^\circ C$ range relevant to processes such as dolomitization (Ferry et al., 2011), burial diagenesis (Huntington et al., 2011), and hydrothermal fluid flow (Bristow et al., 2011). Measurements of clumped isotope compositions of marbles and carbonatites give apparent clumped isotope temperatures in the range of ~ 150–$250\ ^\circ C$, which are interpreted as closure temperatures attained during cooling (Dennis and Schrag, 2010; Schmid and Bernasconni, 2010). (Note that in this paper we use the term 'apparent equilibrium temperature' instead of 'closure temperature', because the system we are studying is closed throughout the cooling process, and does not involve closure of previously open systems during cooling; see Zhang, 1994.) Dennis and Schrag (2010) showed that the slowly cooled Chilwa Isalnd (Malawi) carbonatite has lower apparent equilibrium temperatures than other, presumably

* Corresponding author. Tel.: +1 410 516-4271.
  E-mail address: bhpassey@jhu.edu (B.H. Passey).

faster-cooling carbonatites, but the sensitivity of apparent equilibrium temperature to cooling rate is essentially unknown. For useful high-temperature paleothermometry, it is essential that this sensitivity is characterized. For example, will a hydrothermal calcite precipitated at 300 °C retain a clumped isotopic composition reflective the 300 °C mineralization temperature, or some lower apparent equilibrium temperature?

A related but different motivation for understanding this sensitivity is exploring whether carbonate clumped isotopes constitute a useful system for recording cooling rates. Systems sensitive to cooling rate, 'geospeedometers', have chemical, isotopic, or physical properties that cease to maintain equilibrium below temperature thresholds determined by cooling rate. Geospeedometers are based on mineral texture, diffusive loss of daughter isotopes, diffusive isotope or cation exchange between minerals, homogenization of zoned minerals, and exsolution, as well as homogeneous reactions such as cation order–disorder in pyroxene and reactions involving hydrous species in glass (Zhang, 1994). Most of these systems are based on igneous and metamorphic minerals, and many have apparent equilibrium temperatures in excess of ~400–500 °C. A carbonate clumped isotope 'geospeedometer' based on reaction 1 would be unique in its combination of several attributes: like the cation order/disorder geothermometers, it would be applicable to cooling through relatively low temperatures, and as a homogeneous reaction with unit-cell length scales of diffusion (Dennis and Schrag, 2010), it would be based on a single mineral phase and independent of grain size and geometry. On the other hand, it would be based on isotopic substitutions rather than, for example, exchange of different cations between sites with different electronic environments, so the kinetics might be relatively straightforward. Sample preparation and analysis would be relatively easy, and the method could conceivably be used in any carbonate-bearing rock unit.

This paper presents a first evaluation of the temperature sensitivity of clumped isotope reordering rates. We describe the results of laboratory experiments aimed towards understanding the kinetics of C–O bond reordering in calcite and constraining the Arrhenius parameters for such reordering. We then identify an appropriate analytical solution for apparent equilibrium temperature based on the work of Dodson (1973), and develop a numerical formulation for predicting how clumped-isotope compositions of calcites change in response to scenarios of heating and cooling (or burial and exhumation). We make predictions of relationships between cooling rate and apparent equilibrium temperature, and we use these relationships to estimate cooling rates in two natural systems: the Carrara marble, part of the Alpi Apuane metamorphic core complex that was rapidly exhumed during the late Neogene (Balestrieri et al., 2003), and late Neoproterozoic hydrothermally altered cap carbonates from southern China (Bristow et al., 2011). We conclude with a short discussion of the next steps that will be necessary to fully realize the potential of carbonate clumped isotope geospeedometry.

2. Methods

Experiments were conducted on two different spar calcite samples. MGB-CC-1 is an optical calcite from Minas Gerais, Brazil (Wards Scientific Co.) with a Δ_{47} value of 0.634‰ (the parameter Δ_{47} is defined below). It is suitable for the study of order–disorder kinetics in part because it has a relatively high Δ_{47} value and thus is far from equilibrium Δ_{47} values (ca. 0.30‰) at the reaction temperatures utilized in this study. This provides a maximum change in Δ_{47} in response to diffusive reordering of ~0.34‰ (=0.64–0.30), which is ~20 times larger than the external

precision for clumped isotope analysis (one standard deviation ≈ 0.013‰). The second material, NE-CC-1, is a void-filling spar calcite formed in fluvial sediments of Paleogene age from Nebraska, USA, with a Δ_{47} value of 0.636‰.

Mg, Mn, and Fe compositions of the calcites were measured with the JEOL-JXA-8600 electron microprobe at Johns Hopkins University, with the samples analyzed as crushed mineral grains mounted in epoxy. The optical calcite, MGB-CC-1, is compositionally homogeneous in Mg and Mn, whereas NE-CC-1 is heterogeneous in Mg and Mn (Fig. 1). The latter material is thus not an "ideal" experimental material, but it is plausibly a more realistic representative of natural calcites than the optical calcite. Fe content was below detection limits for both samples (< ~0.01 wt%).

The calcites were crushed in a ceramic mortar and pestle and passed through sieves. The 60–120 mesh (125–251 μm) fractions were collected and rinsed in a sonicator in numerous aliquots of deionized water to remove adhering fine particle material. The materials were dried at 60–70 °C for several hours and stored in a dessicator.

Aliquots of the 60–120 mesh fraction (350 ± 50 μmol $CaCO_3$) were dried under vacuum at 100 °C for 30 min and then and sealed into fused silica tubes along with ~80 μmol dry CO_2. This CO_2 has $\delta^{13}C$ and $\delta^{18}O$ values of −39‰ (PDB) and −31‰ (PDB), respectively, much lower than those of MGB-CC-1 calcite ($\delta^{13}C = -4.8‰$, $\delta^{18}O - 9.3‰$) and NE-CC-1 calcite ($\delta^{13}C = -6.7‰$, $\delta^{18}O - 15.9‰$). Complete isotopic exchange between CO_2 and calcite would change the isotopic compositions of both by several per mil. Thus the isotopically distinct CO_2 provides a means of monitoring for unintended processes during the experimental runs such as decarbonation–carbonation reactions, and solution–precipitation reactions. The samples were held at temperatures ranging from 385 to 800 °C inside of tube furnaces for time periods ranging from 30 min to 44 days, and were then rapidly cooled to room temperature (< 30 s) with a compressed air gun. Temperature was measured with thermocouples and platinum RTDs calibrated by observations of in-vacuo melting points of Sn, Zn, Al, and Ag, as well as the boiling and freezing points of pure water, using ITS 90 reference values (Preston-Thomas, 1990).
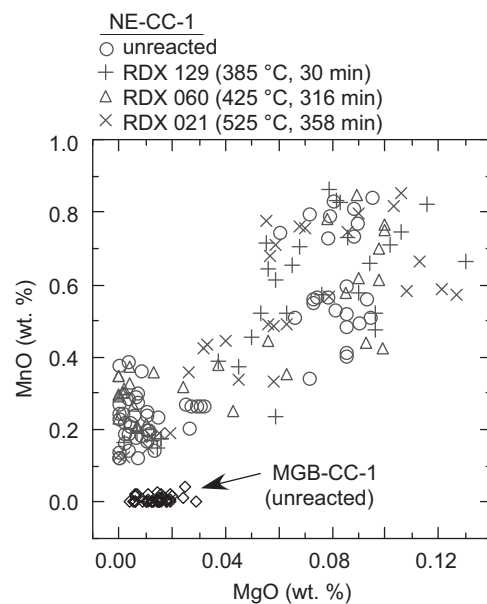

Fig. 1. MnO and MgO contents of the studied calcites based on electron microprobe analysis. Each point reflects an individual microprobe spot analysis, with the analyses performed on many individual grains from the 60–120 mesh size fraction of each material.

These experiments are in the direction of order-to-disorder (i.e., the initially low-T 'ordered' calcites change during heating to a state of less order), whereas cooling and geospeedometry are related to the disorder-to-order direction of clumped isotope reordering. Unfortunately the signal to noise ratio for disorder-to-order experiments is poor. This is because samples with starting compositions at the high T limit have Δ_{47} values that approach the high T asymptote of $\sim$0.27‰ (Fig. 2), whereas equilibrium Δ_{47} values at reaction temperatures suitably high for monitoring reaction progress on laboratory timescales are very similar to the asymptotic value. For example, equilibrium Δ_{47} values at 500 and 300 °C are 0.300‰ and 0.346‰, respectively. Thus the full Δ_{47} signal for a disorder-to-order direction experiment at 300 °C is 0.346–0.270=0.076‰, which is only $\sim$5 times analytical precision ($\sim$0.013‰), and the full signal for a 500 °C experiment is 0.030‰. Thus it is very difficult to accurately characterize reordering profiles for disorder-to-order direction experiments. Therefore our focus was on order-to-disorder experiments, and we conducted only one disorder-to-order direction experiment where samples were preannealed at 700 °C and reacted at 475 °C for different lengths of time. On a theoretical basis, the equilibrium constants for reactions such as Reaction 1 are very close to 1 [on the order of 1.001 or smaller, Schauble et al., 2006]. Thus inasmuch as the equilibrium constant reflects the ratio of the forward and reverse reaction rates, these rates should differ by no more than 1 part in 1000. We therefore proceed assuming that the rates of the order-to-disorder and disorder-to-order reactions are effectively the same at a given temperature.

We conducted two low pressure 'wet' experiments by adding 10 mg of H_2O to reaction tubes otherwise prepared in the same manner as described above. The fused-silica tubes were cut long enough to allow one end of the tube to extend outside of the tube furnace during heating. The cool end of the tube, held at approximately room temperature, limited the pressure of water

to a value corresponding to room temperature (Kronenberg et al., 1984).

We also conducted several wet experiments at 100 MPa. Silver or gold capsules were loaded with $\sim$35 mg NE-CC-1 calcite and 10–20 mg of deionized water. The capsules were welded shut using an H_2+O_2 torch, weighed, placed in an oven (120 °C) for $\sim$1 h, and reweighed to verify that the capsules were tightly sealed. The capsules were then loaded into 9/16″ o.d., 3/16″ i.d. 316 stainless steel reactors (High Pressure Equipment Company 'micro reactors'), pressurized to 100 MPa using water as the pressure medium, and heated at 420 ± 3 °C for periods of time ranging from 124 to 4298 min. Temperature was monitored using thermocouples located inside of the high pressure environment immediately adjacent to the capsules. The experiments were quenched using a compressed air gun, with temperatures falling below $\sim$50 °C in less than 2 min. Pressure was maintained within $\sim$10% of 100 MPa during the heating and cooling intervals, and within $\sim$2% of 100 MPa during annealing at the target temperature, unless otherwise noted.

Stable isotope compositions, including Δ_{47}, were measured at Johns Hopkins University using methods described in Passey et al. (2010). The degree of isotope ordering is measured by Δ_{47}:

$$\Delta_{47} = \left[\left(\frac{R^{47}}{R^{*47}} - 1 \right) - \left(\frac{R^{46}}{R^{*46}} - 1 \right) - \left(\frac{R^{45}}{R^{*45}} - 1 \right) \right] \times 1000 \qquad (2)$$

where R^i=mass i/mass 44 and the asterisk indicates ratios for isotopologues at stochastic abundance levels (Affek and Eiler, 2006).

As developed in Appendix A, we analyze the reaction progress assuming first order kinetics:

$$\ln\left[\frac{\Delta_{47}^t - \Delta_{47}^{eq}}{\Delta_{47}^{init} - \Delta_{47}^{eq}} \right] = \ln\left[1 - \frac{\Delta_{47}^{init} - \Delta_{47}^t}{\Delta_{47}^{init} - \Delta_{47}^{eq}} \right] = \ln[1-F] = -kt \qquad (3)$$

where Δ_{47}^t is the value of the sample held at a temperature T for time duration t and Δ_{47}^{eq} and Δ_{47}^{init} are the equilibrium and initial Δ_{47} values, respectively. k is the reaction rate constant, and F=0 at t=0, and F=1 at equilibrium. Δ_{47}^t and Δ_{47}^{init} are determined directly by mass spectrometry, whereas Δ_{47}^{eq} is estimated from a combination of theory and experiment because equilibrium is not reached on practical timescales at the lower experimental temperatures. The Δ_{47}^{eq} values are based on the lattice dynamics calculations of Schauble et al. (2006), combined with the experimental acid fractionation factor (Δ_{47}^*) measured by Guo et al. (2009), where $\Delta_{47}^{eq} = \Delta_{63}^{eq} + \Delta_{47}^*$. Note that $\Delta_{63} = [(R^{63}/R^{*63}-1) - (R^{62}/R^{*62}-1) - (R^{61}/R^{*61}-1)]*1000$, and R^{*X} is the X/60 ratio for a stochastic abundance of mass X carbonate, and mass 63 is the dominant 'clumped' isotopologue (Schauble et al., 2006). The empirical fractionation factor from Guo et al. (2009), Δ_{47}^*=0.232‰ relative to the 'old' Δ_{47} scale (e.g., Huntington et al., 2009), converts to 0.268‰ on the 'new' scale, using the transfer function in Table 4 of Dennis et al. (2011). Thus we add a constant value of 0.268‰ to the theoretical Δ_{63} values predicted by Schauble et al. (2006). Following Schauble et al. (2006), we express this theoretical temperature calibration for calcite as a 4th order polynomial allowing evaluation at any temperature of interest between 260 and 1500 K:

$$\Delta_{47}^{eq} = \frac{-3.407 \times 10^9}{T^4} + \frac{2.365 \times 10^7}{T^3} - \frac{2.607 \times 10^3}{T^2} - \frac{5.880}{T} + 0.268 \qquad (4)$$

We evaluated these predictions against clumped isotope measurements of calcites driven to equilibrium by heating in dry CO_2 at temperatures between 475 and 800 °C (Fig. 2; data are summarized in Table 1; primary data are given in Tables S1 and S2). We assume that equilibrium has been reached when no further change in Δ_{47} is observed for samples heated for longer periods of time, and the
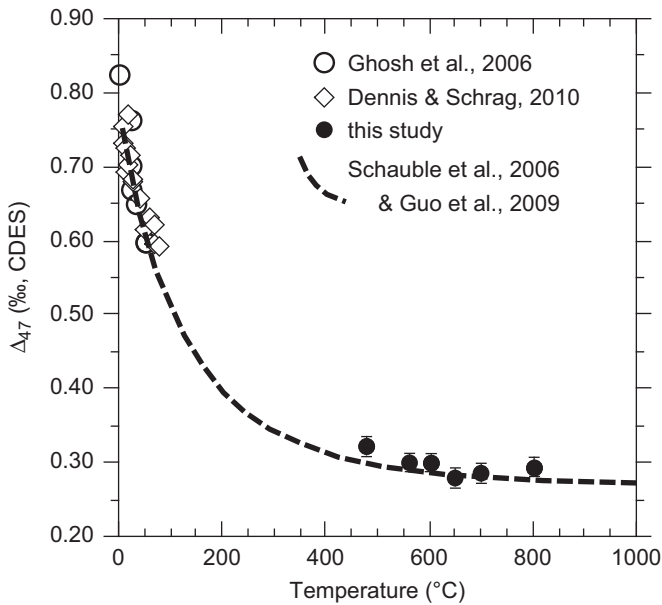
Fig. 2. Theoretical calibration of the carbonate clumped isotope thermometer, adjusted to the 'carbon dioxide equilibrium scale' (CDES) of Dennis et al. (2011) (dashed line, calculated from Eq. (4)). Open symbols show analyses of carbonate precipitated at known temperatures in the laboratory (Ghosh et al., 2006; Dennis and Schrag, 2010), converted to the CDES reference frame using the equations given in Table 4 of Dennis et al. (2011). Filled circles (this study) are calcites driven to clumped isotope equilibrium by prolonged heating at the specified temperature (see text and Table 1).

Table 1
Equilibrium Δ_{63} values for calcite, and predicted and observed Δ_{47} values for CO_2 extracted from calcite, for the experimental temperatures utilized in this study.

T (°C)	Predicted values (Schauble et al., 2006; Guo et al., 2009)		Observed values		'Corrected' values (Eq. 5)
	Δ_{63}, (‰)[a]	Δ_{47}, CDES (‰)[b]	Δ_{47}, CDES (‰)[c]	Residual (‰)	
385	0.050	0.318	–	–	0.330
405	0.045	0.313	–	–	0.325
425	0.041	0.309	–	–	0.321
450	0.037	0.305	–	–	0.317
475	0.033	0.301	0.324	0.023	0.313
560	0.023	0.291	0.302	0.011	0.303
600	0.020	0.288	0.302	0.014	0.300
650	0.016	0.284	0.281	−0.003	0.296
700	0.013	0.281	0.289	0.008	0.293
800	0.009	0.277	0.294	0.017	0.289
			Mean residual	0.012	

[a] Δ_{63} values based on the K_{eq}[$^{13}C^{18}O^{16}O_2$]–temperature relationship reported in Table 6 of Schauble et al. (2006). Values of Δ are calculated from K_{eq} using the approximation $\Delta = 1000 \ln(K_{eq}/K_r)$ (Wang et al., 2004).
[b] CDES: 'carbon dioxide equilibrium scale' proposed in Dennis et al. (2011). This column gives calculated Δ_{47} values of CO_2 extracted from equilibrium carbonate, using the experimental 25 °C acid fractionation factor determined by Guo et al. (2009) (= 0.232‰) converted to the CDES scale (= 0.268‰).
[c] Average values of calcite heating experiments reaching apparent equilibrium, as determined for Δ_{47} values that cease to decrease with longer reaction times. Primary data are given in Tables S1 (475 °C) and S2 (560–800 °C); the experiments used to calculate equilibrium values are as follows: 475 °C: RDX 116, 117, 120; 560 °C: RDX 047, 048; 600 °C: RDX 005, 007, 009; 650 °C: RDX 003, 008, 011; 700 °C: RDX 030; 800 °C: RDX 056, 057. Since these values were measured on CO_2 produced by reaction with phosphoric acid at 90 °C, an acid temperature correction of 0.081‰ was used to normalize the data to the 25 °C scale (Passey et al., 2010).

equilibrium Δ_{47} value is calculated as the average Δ_{47} value for reactions showing no further change in Δ_{47}. The experimental values were on average 0.0116‰ higher in Δ_{47} than the theoretical predictions. We consider these observations to be an improvement to our knowledge of high temperature equilibrium Δ_{47} values, and we apply a +0.0116‰ correction to the predicted values, yielding:

$$\Delta_{47}^{eq} = \frac{-3.407 \times 10^9}{T^4} + \frac{2.365 \times 10^7}{T^3} - \frac{2.607 \times 10^3}{T^2} - \frac{5.880}{T} + 0.280 \tag{5}$$

We use Eq. (5) to predict the Δ_{47}^{eq} values as necessary in the remainder of this study.

3. Results

3.1. MGB-CC-1 optical calcite

The experimental data are reported in Table S1, and are illustrated in Fig. 3. There was no resolvable change in $\delta^{13}C$ and $\delta^{18}O$ values during the course of reaction. The reacted mineral grains have morphology (size, shape, texture, and surface luster) that is indistinguishable from that of unreacted grains, as gauged qualitatively using a binocular microscope. XRD data show no evidence of a change in mineralogy. However, there is a darkening in color of the reacted grains that may indicate pyrolization of trace amounts of organic carbon, or possibly reduction of CO_2 gas to graphite or other reduced carbon. The reaction conditions used here are essentially the same as the low pressure C and O self-diffusion experiments of Labotka et al. (2004), who demonstrated that crystal integrity was preserved even in the outer few tenths
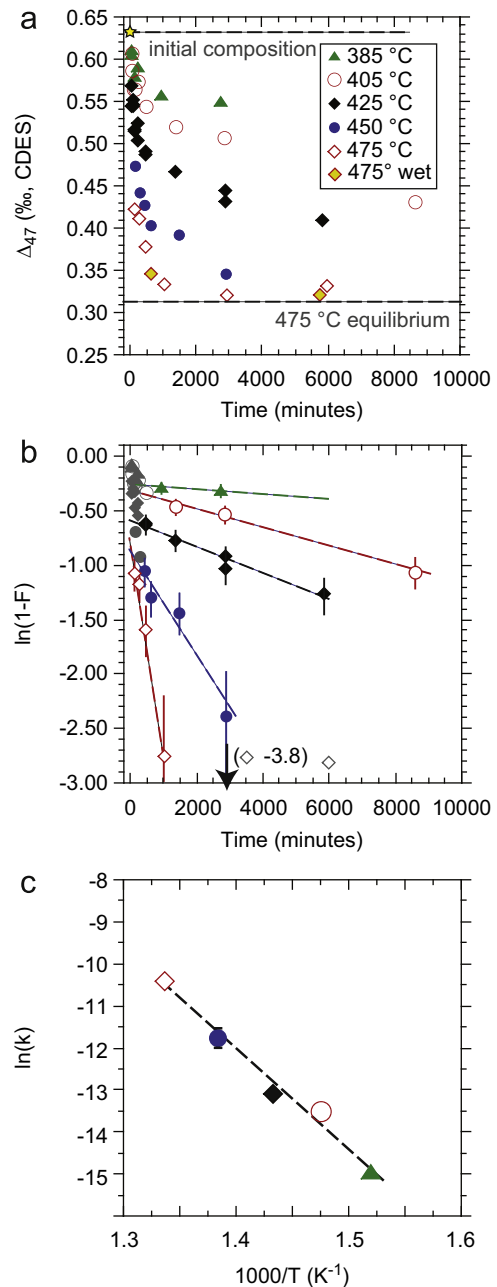

Fig. 3. Results of reordering experiments on optical calcite MGB-CC-1. (a) Evolution of Δ_{47} as a function of time for calcites heated at different temperatures. The symbols labeled 'wet' correspond to reaction tubes with ~10 mg water intentionally introduced to evaluate the effect of water on reordering rates. The initial composition of the mineral is shown by the star. CDES: carbon dioxide equilibrium scale (Dennis et al., 2011). (b) First order reaction progress as a function of time. Grayed symbols correspond to the early non-first order reaction and are not included in the regressions shown by the dashed lines. The open gray diamonds correspond to 475 °C reactions with close approach to equilibrium and hence with data that are not suitable for inclusion in the regression. The slopes of the lines correspond to the negative of the reaction rate constant for each temperature. (c) Arrhenius regression for determining activation energy and frequency factor. The slope of the line is equivalent to $-E_a/R$, and the intercept is equivalent to $\ln(K_o)$. When not visible, error bars are smaller than the symbol size.

of microns of the crystal specimens. Therefore it appears unlikely that the darkening represents significant decomposition of calcite.

The progress of clumped isotope reordering is shown in Fig. 3. The reaction does not follow simple first order kinetics, as the data for each temperature in Fig. 3b do not plot along straight lines intercepting the origin. The reaction proceeds rapidly during

the initial period of heating, and then apparently transitions into first order behavior. We hypothesize that this relates to a period of defect annealing during the early experiment that allows for rapid C–O bond reordering. First order reordering becomes the dominant process following the removal of this 'disequilibrium' defect population, in this case after a few hundred minutes of reaction. Such defect annealing has been demonstrated to influence the results of oxygen self-diffusion experiments in calcite (Kronenberg et al., 1984), and workers studying self-diffusion typically pre-anneal samples at high temperature prior to beginning the actual diffusion experiments in isotopically labeled fluid (e.g. Farver, 1994; Labotka et al., 2004). For clumped isotopes, such preannealing will lead to measureable reordering, and thus the early part of the reactions shown in Fig. 3 can be viewed as 'monitored' pre-annealing. We infer that the initial annealing results from exposure of the starting material to elevated temperatures never experienced during its geologic history. Thus we make the assumption that reordering relevant to geological conditions is given by the first order behavior of the late experimental phase. In this case the slopes of straight lines fitting the late reaction data are equivalent to the negative values of temperature-specific rate constants k, and a fit of the k values to an Arrhenius equation (Fig. 2c) yields the activation energy and frequency factor. Table 2 gives the rate constants and regression information for the dashed line fits shown in Fig. 3b. The activation energy E_a and frequency factor K_o are (see Table 2) $E_a = 197 \pm 19$ kJ/mol and $K_o = 1.4 \ast 10^9$ s^{-1} [$+36 / -1.3 \ast 10^9$].

3.2. NE-CC-1 spar calcite

Clumped isotope data for NE-CC-1 (Table S2) are plotted in terms of reaction progress in Fig. 4a and b. The reacted samples have $\delta^{13}C$ and $\delta^{18}O$ values that are indistinguishable from those of unreacted calcite, except for the 700 and 800 °C reactions, where $\delta^{13}C$ and $\delta^{18}O$ show a small but measurable change of about 0.2‰ or less. The reacted grains exhibit a similar darkening in color as seen in the MGB-CC-1 calcite, although the darkening disappears in the highest temperature reactions.

As with the MGB-CC-1 optical calcite, the change in Δ_{47} for this material does not follow simple first-order kinetics. We surmise that, as with MGB-CC-1, the early reaction is related to a transient period of defect annealing. In addition, it appears that the reaction progress plotted versus time for any one temperature defines two different straight-line segments, an early segment with a steeper slope, and a later segment with a shallower slope (this pattern is most clearly resolved in the 560, 525, and 475 °C data). We observed that this calcite is compositionally heterogeneous in Mg and Mn (Fig. 1), and we hypothesize that the material behaves as a mechanical mixture of two or more components, each with a unique susceptibility to C–O bond reordering. Such behavior is analogous to the decay behavior of a mixture of radioisotopes with different half-lives (e.g., Friedlander et al., 1981) or multi-component isotopic turnover in animals (e.g., Cerling et al., 2007). For a two-component system where each component follows a first order rate law, Eq. (3) becomes:

$$\frac{\Delta_{47}^t - \Delta_{47}^{eq}}{\Delta_{47}^{init} - \Delta_{47}^{eq}} = f_1 e^{-k_1 t} + f_2 e^{-k_2 t} \qquad (6)$$

where f_1 and f_2 are the fractional contributions of the first and second components, and k_1 and k_2 are the rate constants of the first and second components. Appendix B details the 'curve stripping' procedure utilized to determine the rate constants for

Table 2
Rate constant regressions and Arrhenius parameters for reordering reactions in MGB-CC-1 and NE-CC-1 calcite.

T (°C)	Slope ($=-k$) (s^{-1})	Intercept	Fractional contribution	R^2	Stats	RDX points used in regression*
MGB-CC-1 calcite						
385	$-3.18\ (\pm 0.42) \times 10^{-7}$	$-0.27\ (\pm 0.03)$	–	na	na	181, 189
405	$-1.39\ (\pm 0.15) \times 10^{-6}$	$-0.32\ (\pm 0.04)$	–	0.99	a,b,c	169, 173, 177
425	$-2.01\ (\pm 0.15) \times 10^{-6}$	$-0.59\ (\pm 0.02)$	–	0.97	d,e,f	149, 150, 151, 153
450	$-7.95\ (\pm 1.72) \times 10^{-6}$	$-0.88\ (\pm 0.12)$	–	0.91	d,e,f	144, 145, 147, 148
475	$-2.98\ (\pm 0.37) \times 10^{-5}$	$-0.79\ (\pm 0.08)$	–	0.97	d,e,f	112, 113, 114, 115
Arrhenius regression: $E_a = 197 \pm 19$ kJ/mol				0.97	d,e,f	
$K_o = 1.39 \times 10^9$ s^{-1} [$(+36.0 / -1.34) \times 10^9$]						
NE-CC-1 calcite, refractory component						
560	$-1.29\ (\pm 0.05) \times 10^{-5}$	$-1.60\ (\pm 0.02)$	$0.20\ (\pm 0.008)$	0.99	d,e,f	034, 037, 036
525	$-3.66\ (\pm 0.25) \times 10^{-6}$	$-1.47\ (\pm 0.03)$	$0.23\ (\pm 0.014)$	0.99	d,e,f	021, 010, 017, 018, 015
475	$-4.48\ (\pm 0.40) \cdot 10^{-7}$	$-1.06\ (\pm 0.05)$	$0.35\ (\pm 0.036)$	0.98	d,e,f	025, 016, 042, 046
			<u>0.26</u> mean			
Arrhenius regression: $E_a = 200 \pm 2$ kJ/mol				0.99	d,e,f	
$K_o = 4.4 \times 10^7$ s^{-1} [$(+1.4 / -1.0) \times 10^7$]						
NE-CC-1 calcite, labile component						
525	$-1.27\ (\pm 0.13) \times 10^{-4}$	$-1.14\ (\pm 0.06)$	$0.32\ (\pm 0.041)$	–	na	026, 019
475	$-1.63\ (\pm 0.19) \times 10^{-5}$	$-0.74\ (\pm 0.04)$	$0.48\ (\pm 0.038)$	0.95	d,e,f	125, 123, 130, 022, 023, 027, 024
425	$-1.37\ (\pm 0.19) \times 10^{-6}$	$-0.76\ (\pm 0.04)$	$0.47\ (\pm 0.042)$	0.93	d,e,f	065, 060, 064, 061, 063, 062
			<u>0.42</u> mean			
Arrhenius regression: $E_a = 208 \pm 4$ kJ/mol				0.99	d,e,f	
$K_o = 5.6 \times 10^9$ s^{-1} [$(+4.9 / -2.6) \times 10^9$]						

Note: Regressions are error weighted least squares regressions calculated using the statistical software package JMP. $\pm$ values are 1 standard error.
na: statistical tests not applicable.
a: Regression effect significant at the 0.1 level based on ANOVA F-ratio statistic.
b: Slope significantly different than zero at 0.1 level based on Student's t-distribution.
c: Intercept significantly different than zero at 0.1 level based on Student's t-distribution.
d: Regression effect significant at the 0.05 level based on ANOVA F-ratio statistic.
e: Slope significantly different than zero at 0.05 level based on Student's t-distribution.
f: Intercept significantly different than zero at 0.05 level based on Student's t-distribution.
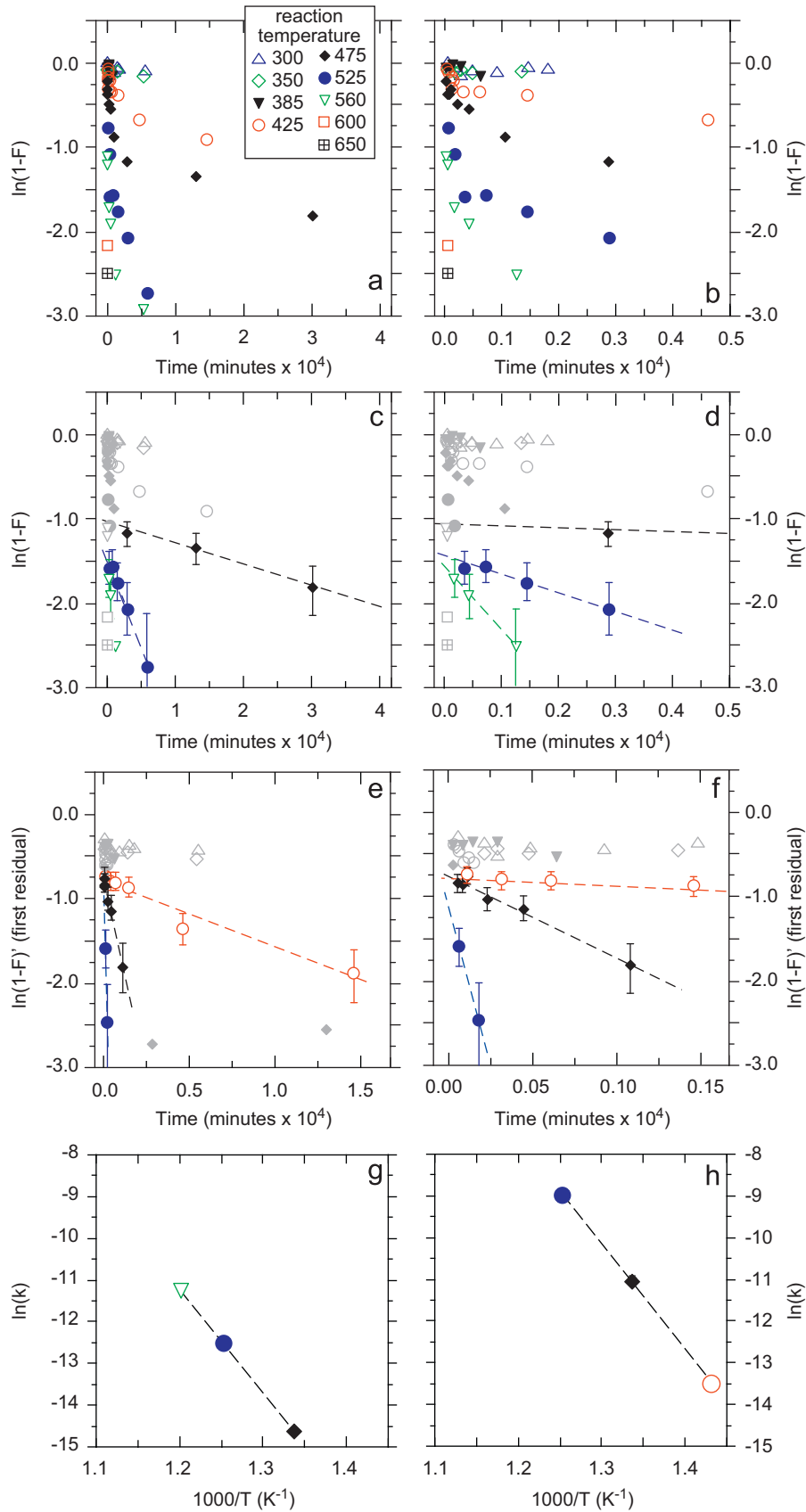   *: Isotope data are given in Tables S1 and S2.

Fig. 4. Results of reordering experiments on spar calcite NE-CC-1. (a) Reaction progress plotted as a function of time. (b) Same as (a), but showing detail of the early reaction. (c) Rate constant regressions corresponding to a refractory component of the mineral. (d) Same as (c), but showing detail of the early reaction. (e) First residual plot showing the data after the influence of the refractory reordering component has been mathematically removed (see Appendix B). Dashed lines show the rate constant regressions for the 'labile' component of the mineral. (f) Same as (e), but showing detail of the early reaction. (g, h) Arrhenius regressions on the refractory and labile components, respectively. Errors are smaller than the symbol sizes.

each component, and Table 2 reports the rate constants and regression information. The resulting Arrhenius parameters are, for the first component: $E_a = 200 \pm 2$ kJ/mol and $K_o = 4.4*10^7$ s^{-1} [$+1.4/-1.0*10^7$], and for the second component: $E_a = 208 \pm 4$ kJ/mol and $K_o = 5.6*10^9$ s^{-1} [$+4.9/-2.6*10^9$]. Thus the activation energies for these two components are similar to each other, and to the activation energy of the optical calcite (197 ± 19 kJ/mol), while the frequency factors differ considerably, spanning a range of $\sim 10^2$.

3.3. Wet versus dry reactions

Low pressure wet experiments conducted on MGB-CC-1 reacted at 475 °C for durations of 631 and 5757 min did not exhibit markedly different rates of reordering compared to the dry experiments (Table S1, Fig. 3). Fig. 5 shows the results of the high-pressure (100 MPa) wet experiments performed on NE-CC-1 at temperatures of 420–422 °C, and the data for these experiments are reported in Table S3. There is no clear difference in reaction rate between dry, low pressure reactions, and wet, high pressure reactions. This is somewhat surprising given that rates of oxygen self-diffusion in calcite are higher under wet, high pressure conditions than under dry, low pressure conditions (e.g., Farver, 1994), and we discuss implications of this result in Section 6 in the context of ideas recently put forward by Labotka et al. (2011).

3.4. Disorder-to-order direction experiments

Several aliquots of NE-CC-1 were heated at 700 °C for 1208 min to drive Δ_{47} values to high-temperature equilibrium, and were then reacted at 475 °C for differing lengths of time (Table S2, Fig. S1). Thus the sense of reordering in these experiments is from a state of less order (less 'clumping') to more order (more clumping). In general, samples reacted for longer periods of time have higher Δ_{47} values than the initial 700 °C annealed material, and the reaction progress (Fig. S1b) is not clearly different from that of the order-to-disorder direction experiments at the same temperature. The reaction progress however is poorly resolved owing to the unfavorable signal to noise ratio and hence there are large uncertainties for these experimental results. These results are consistent with, but do not prove, that order-to-disorder and disoder-to-order reaction rates are the same.

4. Carbonate clumped isotope apparent equilibrium temperature

The geochronological closure temperature is the temperature of the system at the time corresponding to its apparent age (Dodson, 1973). We suggest that the analogous definition for the carbonate clumped isotope apparent equilibrium temperature is the temperature of the system at the time when the equilibrium state of clumped isotope ordering corresponds to the final state of ordering of the system. Fig. 6 illustrates this situation where Δ_{47} is the measure of the state of clumped isotope ordering. A more straightforward and still rigorous definition of apparent equilibrium temperature is the temperature recorded by the clumped isotope composition of a carbonate that has undergone reordering of carbon and oxygen during cooling after crystallization (Ferry et al., 2011).

Since clumped isotope reordering is a distributed process occurring throughout the mineral volume at length scales far shorter than typical mineral grain sizes, there is no grain geometry term in a carbonate clumped isotope apparent equilibrium temperature expression. We argue that the mathematics for clumped isotope apparent equilibrium temperature are analogous to those for geochronological closure temperature where the escape of the daughter isotope is proportional to the concentration of the daughter isotope (the 'first order loss' formulation of Dodson, 1973). In the following discussion we use the somewhat unconventional phrase 'production of disequilibrium' in lieu of 'departure from equilibrium', as usage of the former maintains a consistent temporal directionality in the analogy with a radiogenic system. In the clumped isotope system, the 'production of disequilibrium' is analogous to the production of daughter isotopes (where disequilibrium is the difference between the equilibrium clumped isotope distribution at a given T and the actual clumped isotope distribution of the mineral at that T). The removal of disequilibrium (or the attainment of equilibrium) is analogous to the escape of daughter isotopes from the mineral: at high temperature, the rate of solid-state C–O reordering is sufficiently high to prevent the buildup of disequilibrium in a cooling crystal, just as in the geochronological case the diffusive loss of daughter isotopes is sufficiently rapid to prevent buildup of daughter isotopes. As the system cools through the apparent equilibrium temperature, disequilibrium begins to accumulate, and it continues to accumulate through the remainder of the cooling pathway. Fig. 6 illustrates this concept.
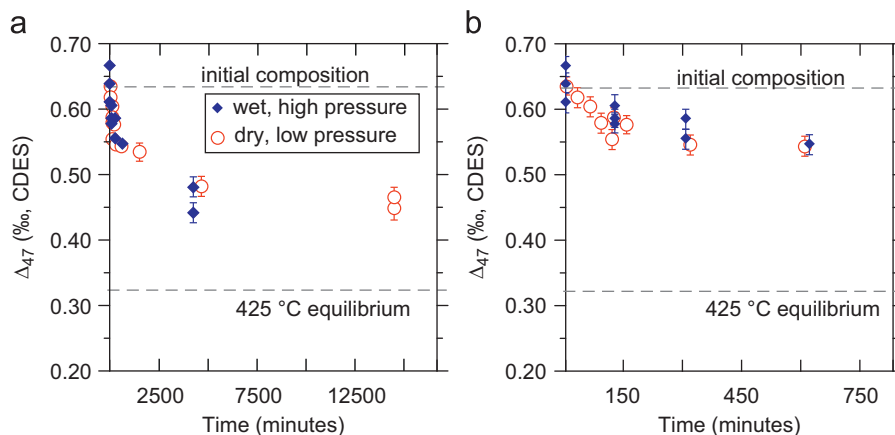
Fig. 5. Comparison between wet high pressure reordering reactions and dry low pressure reactions, both conducted on NE-CC-1 calcite. (a) Blue diamonds show the results for wet high pressure reactions conducted in pure water at a pressure of 100 MPa at a temperature of 400–422 °C. Red circles are the results of dry low pressure reactions conducted at 425 °C under CO_2 gas inside of quartz tubes. (b) Same as (a), but showing detail of early reaction. (For interpretation of the references to color in this figure legend, the reader is referred to the web version of this article.)

Fig. 6. Illustration of apparent equilibrium temperature for carbonate clumped isotopes. (a) Temperature decrease through time, where T^{-1} increases at a constant rate. The horizontal dashed line correspo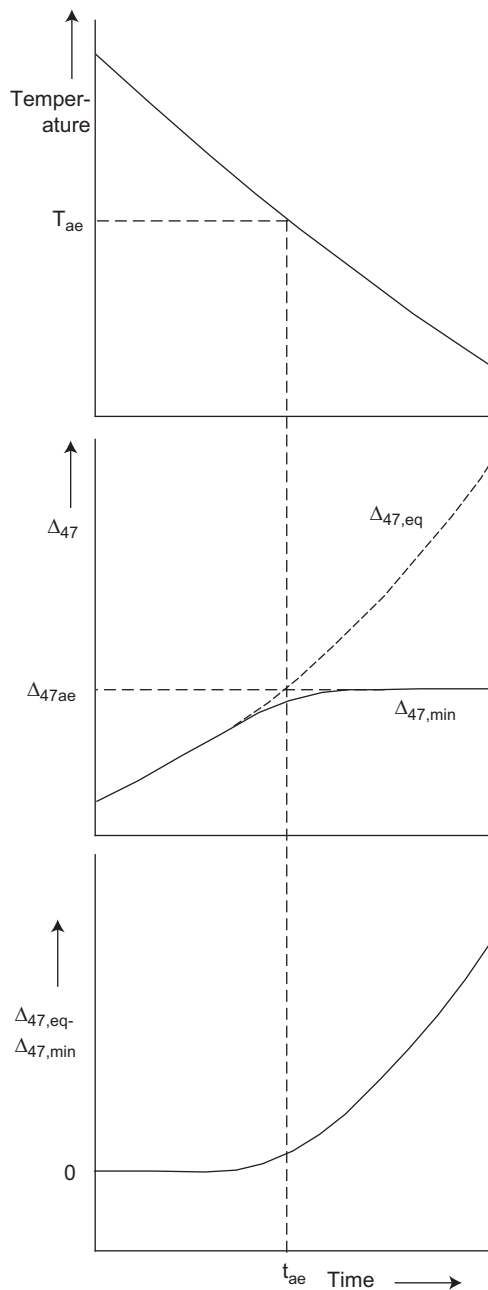nds to the apparent equilibrium temperature T_{ae}. (b) The evolution of the mineral Δ_{47} ($\Delta_{47,min}$, thick curved line) and the equilibrium Δ_{47} ($\Delta_{47,eq'}$, thin dashed curved line). The horizontal dashed line corresponds to the apparent equilibrium composition $\Delta_{47,ae}$, and the vertical dashed line corresponds to the apparent equilibrium time t_{ae}. (c) The evolution of clumped isotope disequilibrium (thick curved line). The horizontal part of the curve represents the part of the cooling history where temperatures are high enough for solid-state reordering to prevent accumulation of disequilibrium.

Clumped isotope disequilibrium can be expressed as $x = \Delta_{47,eq} - \Delta_{47,ccr}$, where $\Delta_{47,eq}$ is the equilibrium Δ_{47} value for a given T, and $\Delta_{47,ccr}$ is the value of a sample cooling at a constant rate in T^{-1} at the same T. The production rate of potential disequilibrium is $p = d\Delta_{47}^{eq}/dT^{-1} \times dT^{-1}/dt$, which can be approximated as constant (note that we use inverse temperature because Dodson's formulation for closure temperature, which becomes

important below, assumes constant cooling in $1/T$). Thus we have:

$$dx/dt = p - k(t)x \tag{7}$$

for first order C–O bond reordering kinetics, where $k(t) = K_o \exp(-E_a/RT)$, and T is a function of t specified by the cooling rate. k, K_o, and E_a are the experimentally derived rate constant and Arrhenius parameters for C–O reordering. The potential disequilibrium is produced by the cooling of the mineral, and the assumption of a constant production rate p is justified because the temperature sensitivity of Δ_{47}^{eq} to T departs only slightly from linear in the narrow temperature interval during closure. Eq. (7) is of the same form as Eq. (4) of Dodson (1973): $dx/dt = \lambda_x c_p - k(t)x$, where $\lambda_x c_p$ is the production of daughter isotopes ($=$decay constant multiplied by the parent isotope abundance) and is assumed to be constant over the "closure" temperature interval, and $-k(t)x$ is the first-order loss of daughter isotopes. We do not repeat the derivation here, but Dodson (1973, p. 262–263, Eq. (14)) shows that the closure temperature expression for this case is

$$\frac{E_a}{RT} = \ln(\gamma \tau K_o) \tag{8}$$

where R is the gas constant, T is the closure temperature, and γ is a constant ($=1.78$). For clumped isotopes we call this temperature the apparent equilibrium temperature (T_{ae}) instead of the closure temperature. Dodson (1973) defined the time constant τ as the time duration over which the rate constant (or diffusion coefficient) decreases by a factor of e^{-1} for a system cooling at a constant rate in T^{-1}:

$$\tau = -RT^2/(E_a dT/dt) \tag{9}$$

As with closure temperature equations, Eqs. (8) and (9) are iterative in T and converge to the apparent equilibrium temperature T_{ae} after a few iterations. In addition, although the mathematics are exact only for cooling at a constant rate in T^{-1}, the computed T_{ae} is accurate for a constant rate of cooling in T.

The apparent equilibrium temperature can also be determined numerically. A common form of the Arrhenius equation is

$$k_T = K_o \exp(-E_a/RT) \tag{10}$$

which is equivalent to

$$k_T = k_{ref} \exp\left[\frac{E_a}{R}\left(\frac{1}{T_{ref}} - \frac{1}{T}\right)\right] \tag{11}$$

when $T_{ref} = \infty$. The determination of K_o as the intercept in a regression of $\ln(k)$ versus $1/T$ (e.g., Fig. 3c) requires an extrapolation far outside of the experimental range of temperatures, resulting in a large error for K_o. To avoid this error, one may instead choose a reference temperature falling within the range of experimental temperatures and utilize Eq. (11) in favor of Eq. (10). Appendix C describes the scheme we used for selecting T_{ref} and k_{ref}. Combining Eqs. (3) and (11) yields

$$\ln\left[\frac{\Delta_{47}^t - \Delta_{47}^{eq}}{\Delta_{47}^{init} - \Delta_{47}^{eq}}\right] = -t k_{ref} \exp\left[\frac{E_a}{R}\left(\frac{1}{T_{ref}} - \frac{1}{T}\right)\right] \tag{12}$$

This equation can be adapted to numerical modeling as

$$\Delta_{47}^i = \left(\Delta_{47}^{i-1} - \Delta_{47}^{eq,i}\right)\exp\left\{-\Delta t k_{ref}\exp\left[\frac{E_a}{R}\left(\frac{1}{T_{ref}} - \frac{1}{T}\right)\right]\right\} + \Delta_{47}^{eq,i} \tag{13}$$

where the cooling rate for any step of the model is $(T_i - T_{i-1})/\Delta t$, Δ_{47}^i is the value of the mineral at time step i, $\Delta_{47}^{eq,i}$ is the equilibrium value at i, and $i-1$ is the preceding time step. This model is run with progressively decreasing temperature until Δ_{47}^i ceases to evolve, at which point Δ_{47}^i corresponds to the apparent equilibrium Δ_{47} (and corresponding apparent equilibrium temperature). The apparent equilibrium Δ_{47} values determined

numerically agree with the analytical values (Eqs. (8) and (9)) within ~0.002‰, with some of the offset due to the use of k_{ref} in the numerical formulation and K_o in the analytical formulation. An advantage of a numerical approach is that Eq. (13) allows for modeling of Δ_{47} evolution in response to any T-t history, including complex scenarios of heating and cooling.

5. Geospeedometry and the cooling rate of Carrara marble and Doushantou cap carbonates

Eqs. (8) and (9) can be combined with the Arrhenius relation (Eq. (10)) to give

$$dT/dt = \frac{\gamma RT_{ae}^2 k_{Tae}}{E_a} \qquad (14)$$

where dT/dt is in °C/s, and k_{Tae} is the rate constant at T_{ae}. Eq. (14) is essentially the approximation given by Zhang (1994) for first order homogeneous reactions, and differs only in a constant, which is 2 in Zhang's equation ($\gamma = 1.78$ here). In practice, T_{ae} is given by the measured Δ_{47} of the sample, converted to T using a calibration such as Eq. (5), E_a is experimentally determined, and k_{Tae} is calculated from the experimentally determined E_a and k_{ref} using Eq. (11). Appendix C describes the error propagation for determining the uncertainty in cooling rate given uncertainties in Arrhenius parameters and measurement error in Δ_{47}. If the kinetics of a mineral are known to the same degree of certainty as the calcites studied here, the uncertainty in reconstructed cooling rates will be on the order of a factor of 5 or better for a range of cooling rates (Table 3). However, each calcite in this study defines a different cooling rate/apparent equilibrium temperature curve (Fig. 7), and the inferred cooling rates range over about two to three orders of magnitude for any particular apparent equilibrium temperature. Therefore, assuming the calcites studied here span the natural range of variability in kinetics, the uncertainty in cooling rate for a material with unknown kinetics would be about ±1–3 orders of magnitude. However, this is a weak assumption given that reordering behavior has been characterized for only two calcites.

Carrara marble has a well constrained cooling history and serves as the first test of the predicted apparent equilibrium temperature/ cooling rate relationships. Carrara marble, part of the Alpi Apuane metamorphic core complex in the Northern Apennines, Italy, is culturally famous from its long use in sculpture and architecture. The Mesozoic parent limestone of Carrara marble was heated to temperatures exceeding 350 °C

during the late Oligocene to middle Miocene as a result of tectonic overthrusting (Carmignani and Kligfield, 1990). Cooling began in the late Miocene during rapid exhumation of the metamorphic core, as documented by a series of thermochronometers (Fellin et al., 2007; Balestrieri et al., 2003). K–Ar and ^{40}Ar/^{39}Ar dates on white micas (closure temperature ~350 °C) are ~8–10 Ma (Kligfield et al., 1986), fission track ages in zircon (closure temperature ~250 °C) are ~10–11 Ma, U–Th/He ages in zircon (closure temperature ~200 °C) are ~5–7.5 Ma (Balestrieri et al., 2003), and fission track ages in apatite (closure temperature ~120 °C) are ~2.5–5.5 Ma (Carmignani and Kligfield, 1990; Balestrieri et al., 2003). Given these constraints, cooling rates estimated by Balestrieri et al. (2003) are, assuming linear cooling between the closure temperatures of pairs of thermochronometers, 10–16 °C/Ma for cooling between 250 and 200 °C, and 38–55 °C/Ma for cooling between 200 and 120 °C.

The mean Δ_{47} value of three different Carrara marble 'in house' standards analyzed in four different laboratories as part of an intercalibration exercise is 0.395‰ with a standard error of 0.004‰ (Dennis et al., 2011). This corresponds to an apparent equilibrium temperature of 222 ± 6 °C (based on Eq. (5)). The corresponding cooling rates based on clumped isotopes calculated
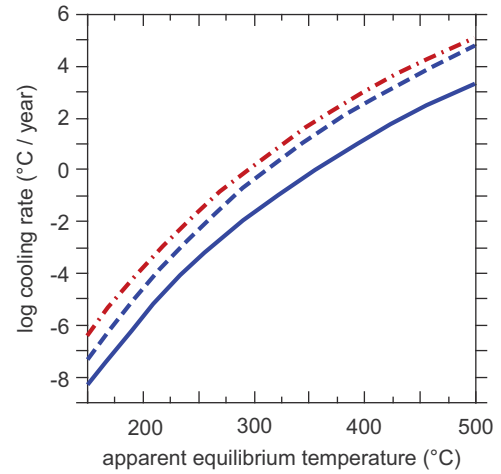

Fig. 7. Relationship between cooling rate and apparent equilibrium temperature for the three different sets of Arrhenius parameters derived in this study. Red dot-dashed line: MGB-CC-1 (optical calcite). Blue dashed line: NE-CC-1 labile component. Blue solid line: NE-CC-1 refractory component. (For interpretation of the references to color in this figure legend, the reader is referred to the web version of this article.)

Table 3
Carbonate clumped isotope closure closure temperatures and the equivalent cooling rates that would be inferred for materials with the kinetics of MGB-CC-1, NE-CC-1 labile component, and NE-CC-1 refractory component.

Closure T (°C)	Closure Δ_{47} (‰) (CDES)*	Cooling rate (°C/yr)		
		MGB-CC-1	NE-CC-1 (refractory)	NE-CC-1 (labile)
500	0.298	1.0×10^5 ($\times 4.9 \div 5.2$)	1.9×10^3 ($\times 4.8 \div 5.0$)	6.2×10^4 ($\times 5.1 \div 5.3$)
450	0.305	1.1×10^4 ($\times 4.1 \div 4.3$)	1.9×10^2 ($\times 4.1 \div 4.2$)	5.8×10^3 ($\times 4.3 \div 4.4$)
400	0.314	8.2×10^2 ($\times 3.5 \div 3.6$)	1.4×10^1 ($\times 3.5 \div 3.5$)	3.8×10^2 ($\times 3.7 \div 3.7$)
350	0.327	4.2×10^1 ($\times 3.2 \div 3.3$)	6.8×10^{-1} ($\times 3.0 \div 3.0$)	1.7×10^1 ($\times 3.1 \div 3.2$)
300	0.344	1.3×10^0 ($\times 3.3 \div 3.4$)	2.0×10^{-2} ($\times 2.6 \div 2.6$)	4.2×10^{-1} ($\times 2.8 \div 2.8$)
275	0.354	1.8×10^{-1} ($\times 3.6 \div 3.7$)	2.7×10^{-3} ($\times 2.4 \div 2.5$)	5.3×10^{-2} ($\times 2.6 \div 2.6$)
250	0.367	2.0×10^{-2} ($\times 3.9 \div 4.0$)	3.0×10^{-4} ($\times 2.2 \div 2.3$)	5.4×10^{-3} ($\times 2.4 \div 2.4$)
225	0.382	1.9×10^{-3} ($\times 4.6 \div 4.7$)	2.7×10^{-5} ($\times 2.1 \div 2.1$)	4.4×10^{-4} ($\times 2.3 \div 2.3$)
200	0.399	1.4×10^{-4} ($\times 5.6 \div 5.8$)	1.9×10^{-6} ($\times 2.1 \div 2.1$)	2.8×10^{-5} ($\times 2.3 \div 2.3$)
175	0.420	7.6×10^{-6} ($\times 7.1 \div 7.4$)	9.9×10^{-8} ($\times 2.0 \div 2.0$)	1.3×10^{-6} ($\times 2.3 \div 2.3$)
150	0.445	3.0×10^{-7} ($\times 9.3 \div 9.8$)	3.7×10^{-9} ($\times 1.9 \div 1.9$)	4.4×10^{-8} ($\times 2.2 \div 2.2$)

Note: ± values were calculated as described in Appendix C, and are based on a standard error in Δ_{47} of 0.005‰.

* CDES: carbon dioxide equilibrium scale (Dennis et al., 2011).

using Eq. (14) are 1410 °C/Ma ($\times 4.4$, $\div 4.6$), 324 °C/Ma ($\times 1.4$, $\div 1.4$), and 19.7 °C/Ma ($\times 1.2$, $\div 1.2$), for the kinetics of MGB-CC-1, NE-CC-1 labile component, and NE-CC-1 refractory component, respectively (where k_{Tae} is calculated using Eq. (11)). The calculated cooling rates have a moderate dependence on the Δ_{47}–T relationship used to calculate apparent equilibrium temperatures: if Eq. (4) is used instead of Eq. (5) (which amounts to a 0.0116‰ 'shift' in the Δ_{47}—T curve, see 'Methods'), the calculated apparent equilibrium temperature is 206 ± 6 °C, corresponding to cooling rates of 267 °C/Ma ($\times 5.1$, $\div 5.2$), 56 °C/Ma ($\times 1.5$, $\div 1.5$), and 3.6 °C/Ma ($\times 1.2$, $\div 1.2$), for the kinetics of MGB-CC-1, NE-CC-1 labile component, and NE-CC-1 refractory component, respectively. Thus, while there is some overlap in cooling rates estimated from clumped isotopes and those estimated by thermochronology, the former range over 2–3 orders of magnitude. This can conceivably be reduced with better defined Δ_{47}–T relationships, and with a better understanding of Arrhenius parameters for reordering of natural calcites. We note that compositionally there is essentially no overlap among Carrara marble and MGB-CC-1 and NE-CC-1. For example, Carrara marble is elevated in MgO (~ 2.8 wt%) and has very little MnO (< 0.003 wt%) (Herz and Dean, 1986), whereas MGB-CC-1 has less than 0.02–0.03 wt% MgO and no detectable MnO, and NE-CC-1 has < 0.13 wt% MgO and 0.1–0.9 wt% MnO (Fig. 1). Texturally the NE-CC-1 and Carrara marble are more similar to each other than to the optical calcite MGB-CC-1.

Bristow et al. (2011) studied ^{13}C-depleted calcites from the late Neoproterozoic Doushantou cap carbonate (South China) and reported the highest observed carbonate clumped isotope temperatures for natural calcites to date, 476 ± 77 °C. The inferred cooling rates based on the carbonate clumped isotope geospeedometer are 36,000 °C/annum ($\times 26$, $\div 86$), 21,000 °C/a ($\times 31$, $\div 96$), and 650 °C/a ($\times 27$, $\div 67$), based on the kinetics of MGB-CC-1, NE-CC-1 labile, and NE-CC-1 refractory, respectively. The ^{13}C-depleted calcites studied by Bristow et al., 2011 are enriched in Mn ($\sim 11,000$ ppm) and low in Mg, and thus are compositionally more similar to NE-CC-1 than to MGB-CC-1. Despite the wide range of cooling rates inferred for these calcites, it appears that cooling of the Doushantou ^{13}C-depleted calcites was extremely rapid, consistent with growth during very short-lived hydrothermal activity, as hypothesized by Bristow et al. (2011), and inconsistent with a slow rate of temperature change during regional metamorphism.

6. Discussion

Results of this study demonstrate that different carbonates can have different susceptibilities to ^{13}C-^{18}O bond reordering. Inasmuch as solid-state diffusion is enabled by lattice defects, we infer that the susceptibility to reordering for any particular carbonate mineral will be a function of the defect ensemble of the mineral. The overall contribution to C–O reordering by any one kind of defect will be related to its concentration, mobility through the mineral lattice, and efficacy at causing the breakage of existing C–O bonds and replacement of C and O atoms as a new C–O bond reforms. These defects will include intrinsic defects with thermodynamically controlled abundances such as Frenkel vacancy-interstitial pairs, as well as extrinsic defects related to cation substitutions and presence of trace elements. In addition, the inherent mobility of any defect type might be limited by traps or physical barriers such as dislocations and grain boundaries.

It may be significant that the three measured activation energies are broadly similar, all falling within the range of 197–208 kJ/mol, whereas the frequency factors range over about two orders of magnitude. This may indicate that C–O reordering in both minerals is caused by the same kinds mechanisms and hence

similar kinds of defects, but that these defects differ in concentration, or mobility, or both. The NE-CC-1 calcite, with its high concentration of Mn and Mg, and poor optical transparency, is expected to have a higher overall defect concentration than the optical calcite (MGB-CC-1). Thus it is somewhat surprising that the frequency factor of the 'refractory' component of NE-CC-1 is more than twenty times lower than that of MGB-CC-1, while the frequency factor of the 'labile' component is about four times higher than of MGB-CC-1. Thus there appears to be decoupling between frequency factor and overall defect concentration. This may indicate an importance of larger-scale defect structures in trapping and pinning 'active' defects, impeding their transit through the mineral volume and thus impeding C–O reordering. Under such a scenario, the optical calcite, with very few grain boundaries and other large-scale defect structures, would be highly permeable to defects. Stated differently, the optical mineral contains few structures capable of impeding the random-walk of migrating point defects. Thus the optical calcite has a high frequency factor and high susceptibility to C–O bond reordering. In this model, the two components of the NE-CC-1 calcite may represent two different types of intracrystalline domains, with the labile component (with the higher frequency factor) having the higher optical quality than the refractory component (with the lower frequency factor). This is consistent with the nature of the material, which derives from many different crystals from the same hand sample of sedimentary rock, with the crystals having differing degrees of optical quality. We note also that preliminary experimental data from a micritic soil carbonate reacted at 425 °C shows a similar pattern of reordering as NE-CC-1 reacted at the same temperature, both of which have much lower reaction rates than MGB-CC-1 reacted at the same temperature.

Thus, we envision that a useful avenue for future research is to study how susceptibility to C–O reordering varies as a function of optical quality or other measures lattice domain size and continuity. A separate line of research could investigate how susceptibility varies as a function of trace and minor element concentrations in minerals of similar optical quality. A third line of research could study reordering rates in carbonates with different major cations, such as $CaMg(CO_3)_2$, $MgCO_3$, $FeCO_3$, $MnCO_3$, $SrCO_3$, $PbCO_3$. At any rate, the full potential of a carbonate clumped isotope 'geospeedometer' will only be realized with a good understanding of the predominant controls on susceptibility to C–O reordering.

We observed that water and pressure seem to have little influence on rates of C–O reordering. This contrasts with the well-established finding that rates of O self-diffusion in calcite (and many other minerals) are accelerated in the presence of water, with the effect proportional to H_2O fugacity (e.g., Kronenberg et al., 1984; Farver 1994). However, Labotka et al. (2011) have recently argued that the mechanism of enhanced oxygen self-diffusion under wet, high pressure conditions in calcite relates to heterogeneous reactions at the calcite surface, where interactions between H_2O, H^+, and OH^- and unsatisfied charges at the calcite surface result in the creation of lattice vacancies. These vacancies, concentrated in the near-surface region, lead to enhanced O exchange between mineral and fluid, but do not change the diffusivity of the bulk mineral aside from the near-surface region. In addition, Labotka et al. (2011) did not observe increased concentrations of H inside of the mineral, which argues against the hypothesis that free H (supplied by the water) diffuses rapidly into the mineral volume and increases the inherent diffusivity of mineral. The absence of a measureable dependence of rates of clumped isotope reordering on water pressure supports the conclusion of Labotka et al. (2011) that the enhancement of O self-diffusion by H_2O is a surficial rather than volume phenomenon.

7. Conclusions

This study presents the first measurements of the kinetics of ^{13}C–^{18}O bond reordering in calcite. We find that different calcites have different susceptibilities to C–O bond reordering, and that reaction progress seems to follow a first order rate law, but only after an initial period of defect annealing. We suggest that this initial annealing is an experimental artifact of rapid heating of minerals that have never been exposed to high-T conditions, and therefore irrelevant to measuring the cooling rates of natural calcite samples crystallized at, and cooling from, high T. Assuming first order kinetics, we present equations based on the work of Dodson (1973) for determining apparent equilibrium temperatures as a function of cooling rate (Eqs. (8) and (9)), as well as an equation for determining cooling rate when the apparent equilibrium temperature is known (Eq. (14)). For samples with cooling rates that are approximately constant through the apparent equilibrium temperature, the temperature corresponding to the Δ_{47} value of the sample is the apparent equilibrium temperature. We also present a numerical formulation that allows modeling of the evolution of Δ_{47} of a sample in response to any temperature history.

These conclusions rely chiefly on three assumptions which should receive further scrutiny. First, C–O bond reordering follows a first order rate law; second, the order-to-disorder process (i.e., reordering from low temperature to high temperature) has the same rate at a given temperature as the disorder-order process (reordering from high to low temperature); and third, the mechanisms of reordering in the high T laboratory experiments are the same as those operating at the lower temperatures where closure occurs for many geological materials.

Nevertheless, the results presented here suggest that the carbonate clumped isotope system is capable of recording cooling rates. If the Arrhenius parameters of the specimen in question are well known or can be modeled, the cooling rate of that specimen can be inferred within a factor of $\sim$5 or better. The main limitation to accurate estimates of cooling rates will be accurately defining the Arrhenius parameters for specific study materials. This in turn will hinge upon identification and modeling of relationships between Arrhenius values and macroscopic mineral properties, or as yet unforeseen ways of probing reordering characteristics of natural study materials with Δ_{47} values close to the high temperature asymptote. This is analogous to the idea presented by Reiners et al. (2005) that thermochronometric methods could be greatly enhanced by methods to identify and exploit the unique diffusive characteristics of individual samples—to determine the kinetics of each sample rather than assume a generic behavior. The fact that different calcites will have different reordering characteristics is a circumstance that could work to an advantage if the differences can be appreciated and well understood. For example, rock units with multiple compositions of carbonate could effectively contain multiple geothermometers with closure at different times during the cooling history of the rock.
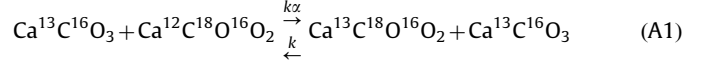
Appendix A. Derivation of the first order rate equation

The reordering reaction can be written as

$$Ca^{13}C^{16}O_3 + Ca^{12}C^{18}O^{16}O_2 \underset{k}{\overset{k\alpha}{\rightleftarrows}} Ca^{13}C^{18}O^{16}O_2 + Ca^{13}C^{16}O_3 \quad (A1)$$

where the reaction from left to right corresponds to the ordering reaction, and from right to left is the disordering reaction. For simplicity in the discussion below, we denote the species in Eq. (A1) as (from left to right) 61, 62, 63, and 60, in reference to the atomic masses of the carbonate ion in each species. Also note that we do not explicitly include ^{17}O and the isotopologues $^{12}C^{17}O^{18}O^{16}O$, $Ca^{13}C^{17}O_2^{16}O$, and $Ca^{12}C^{17}O_3$, which together comprise about 6.5% of mass 63 isotopologues (Ghosh et al. 2006). The following derivation is based on Zhang's approach for homogeneous isotope exchange reactions (Zhang 2008; Section 2.1.2.4). The reaction progress parameter ξ is defined as

$$\frac{d\xi}{dt} = \frac{d[63]}{dt} = \frac{d[60]}{dt} = -\frac{d[61]}{dt} = -\frac{d[62]}{dt} \quad (A2)$$

where the brackets denote fractional abundances ($[60]+[61]+[62]+[63] \approx 1$). ξ is related to the species concentrations as follows:

$$[63] = [63]_0 + \xi$$
$$[60] = [60]_0 + \xi$$
$$[61] = [61]_0 - \xi$$
$$[62] = [62]_0 - \xi \quad (A3)$$

Based on reaction (A1) and Eqs. (A2) and (A3), we have

$$\frac{d\xi}{dt} = k\alpha([61]_0 - \xi)([62]_0 - \xi) - k([63]_0 + \xi)([60]_0 + \xi) \quad (A4a)$$

which is equivalent to

$$\frac{d\xi}{dt} = k(\alpha-1)\xi^2 - k\{\alpha([61]_0 + [62]_0) + [63]_0 + [60]_0\}\xi$$
$$+ k\{\alpha([61]_0[62]_0) - [63]_0[60]_0\}. \quad (A4b)$$

The first term on the right hand side can be ignored because ξ is small and α is close to 1.

We define the following:

$$A = \alpha([61]_0 + [62]_0) + [63]_0 + [60]_0$$
$$B = \alpha([61]_0[62]_0) - [63]_0[60]_0$$

and therefore

$$\frac{d\xi}{dt} = -kA\xi + kB \quad (A5)$$

The solution to this equation is (Zhang, 2008):

$$\xi = \frac{B}{A}\left(1 - e^{-kAt}\right) \quad (A6)$$

Combining (A3) and (A6), and observing that $A \approx 1$ gives

$$\frac{[63] - [60]_0}{\alpha[61]_0[62]_0 - [63]_0[60]_0} = 1 - e^{-kt} \quad (A7)$$

The numerator on the left hand side is approximately equal to $[63]_{eq} - [63]_0$ as demonstrated by the following. The equilibrium constant α is defined as

$$\alpha = \frac{[63]_{eq}[60]_{eq}}{[61]_{eq}[62]_{eq}}, \quad (A8)$$

and by analogy to Eq. (A3) we define:

$$[63]_{eq} = [63]_0 + \chi$$

$$[60]_{eq} = [60]_0 + \chi$$
$$[61]_{eq} = [61]_0 - \chi$$
$$[62]_{eq} = [62]_0 - \chi \tag{A9}$$

Therefore the numerator in Eq. (A7) is equivalent to:

$$\alpha([61]_{eq} + \chi)([62]_{eq} + \chi) - [63]_0([60]_{eq} + \chi) \tag{A10a}$$

or

$$\alpha([61]_{eq}[62]_{eq} + \chi([61]_{eq} + [62]_{eq}) + \chi^2) - [63]_0[60]_{eq} - [63]_0\chi \tag{A10b}$$

We observe that $[61]_{eq} + [62]_{eq} \approx 1 - [60]_{eq}$, and $\chi = [63]_{eq} - [63]_0$. Therefore:

$$\alpha([61]_{eq}[62]_{eq} + ([63]_{eq} - [63]_0)(1 - [60]_{eq}) + \chi^2) - [63]_0[60]_{eq} - [63]_0\chi \tag{A10c}$$

which reduces to (after some algebra and considering Eq. (A8)):

$$\alpha([63]_{eq} - [63]_0) - [63]_0\chi + [60]_{eq}([63]_{eq} - \alpha[63]_{eq} + \alpha[63]_0 - [63]_0) \tag{A10d}$$

Since $\sim 1.001 > \alpha > 1.000$, the right hand term is negligible, and the left hand term is approximately equal to $[63]_{eq} - [63]_0$. In addition, since χ is a very small number, the term $[63]_0\chi$ is negligible in comparison to $[63]_0$. Combining this result with Eq. (A7) gives

$$\frac{[63] - [60]_0}{[63]_{eq} - [63]_0} = 1 - e^{-kt} \tag{A11a}$$

or

$$\frac{[63] - [63]_{eq}}{[63]_0 - [63]_{eq}} = e^{-kt} \tag{A11b}$$

This is equivalent to

$$\frac{\Delta_{63}^t - \Delta_{63}^{eq}}{\Delta_{63}^{init} - \Delta_{63}^{eq}} = e^{-kt}, \tag{A11c}$$

where $\Delta_{63} = [(R^{63}/R^{*63} - 1) - (R^{62}/R^{*62} - 1) - (R^{61}/R^{*61} - 1)]*1000$, and R^{*X} is the $X/60$ ratio for a stochastic abundance of mass X carbonate (Schauble et al., 2006), and where the superscript 'init' is equivalent to the subscript '0' in the previous equations (denoting the initial composition). As a final check, we evaluated the equivalence of Eq. (A11c) and (A7) by inserting isotopologue concentrations calculated for natural abundance carbon and oxygen isotope compositions, and varying ξ over a range of values equivalent to ~ 1.5‰ variation in Δ_{63}; for these conditions, the reaction progress calculated by the two equations differs by $\sim 10^{-5}$ or less.

In practice, Δ_{63} is not measured directly, but rather is approximated by measuring enrichment of $^{13}C^{18}O^{16}O$ in CO_2 generated from carbonate by acid digestion. Thus $\Delta_{63} = \Delta_{47} - \Delta_{47}^*$ (Guo et al., 2009), where Δ_{47}^* is the temperature-dependent acid fractionation. In this study, Δ_{47}^* is treated as a constant for any given temperature of acid digestion of carbonate, although Guo et al. (2009) predict a small dependency of this parameter on the Δ_{63} value of carbonate (~ 0.035‰ for every 1‰ increase in Δ_{63}), the magnitude of which is similar to analytical uncertainty for the range of Δ values encountered in this study (range ≈ 0.34‰, equivalent to 0.012‰ change in Δ_{47}^*). Therefore, Eq. (A11c) can be approximated by the following:

$$\frac{\Delta_{47}^t - \Delta_{47}^{eq}}{\Delta_{47}^{init} - \Delta_{47}^{eq}} = e^{-kt} \tag{A11d}$$

We also define the reaction progress variable F as

$$F = \frac{\Delta_{47}^{init} - \Delta_{47}^{(t)}}{\Delta_{47}^{init} - \Delta_{47}^{eq}} \tag{A12}$$

where $F = 0$ at $t = 0$, and $F = 1$ at equilibrium. Combining Eqs. (A11d) and (A12) and taking natural logs yields:

$$\ln[1 - F] = -kt \tag{A13}$$

Note that these equations have the form of a solution to a rate equation for a first-order chemical reaction. This follows from Eq. (A1) because the only term that changes significantly is [63], and thus [61], [62], and [60] can be treated as constants. Therefore Eq. (A1) describes a pseudo first-order reaction.

A.1. Conceptual basis for first-order rate law

We assume that the mechanisms of reordering are dominated by migration of point defects such as vacancies and interstitials (or vacancy–interstitial pairs such as Frenkel defects), that the concentration of such defects is constant (or becomes constant following the initial annealing of nonequilibrium defects), that the mobility of defects and their efficacy at effecting C–O bond reordering is constant, and that defect migration is a purely random process. These are essentially the same assumptions made in conventional solid-state volume diffusion studies where a diffusion profile is interpreted in the context of the diffusion equation. Therefore from the perspective of any fixed position in the mineral lattice, the flux of defects passing through the position is constant through time. For clumped-isotope reordering reactions to take place, a 'clumped' CO_3 site must be adjacent to an 'unclumped' site and transited by a defect, which causes swapping of C or O to form two singly-substituted CO_3 groups. The probability of a reordering reaction within a finite volume of lattice is therefore proportional to the products of the concentrations of clumped sites, unclumped sites, and the defect flux: $P_R \propto [63][60]\Phi_d$ (where Φ_d is the defect flux). The relative change is [60] as a function of time is small compared to relative changes in [63], so [60] is treated as a constant (as described above). The defect flux Φ_d is also constant, so the reaction is a pseudo-first order reaction for this set of conditions.

Appendix B. Curve stripping approach for identifying multiple components

The model developed here is analogous to a multi-component radioisotope system (e.g., Friedlander et al., 1981) or multiple isotopic turnover pools in biological systems (e.g., Cerling et al., 2007). For multiple component clumped-isotope reordering, Eq. (3) can be generalized as

$$\frac{\Delta_{47}^{(t)} - \Delta_{47}^{eq}}{\Delta_{47}^{init} - \Delta_{47}^{eq}} = \sum f_i e^{-k_i t} \tag{B1}$$

where f_i is the fractional contribution of the ith pool, k_i is the rate constant of the ith pool, and all other parameters are as defined in Section 2. For a two component system where each component follows a first order rate law, (B1) becomes

$$\frac{\Delta_{47}^{(t)} - \Delta_{47}^{eq}}{\Delta_{47}^{init} - \Delta_{47}^{eq}} = f_1 e^{-k_1 t} + f_2 e^{-k_2 t}. \tag{B2}$$

If $k_2 \ll k_1$, then at sufficiently long t the first terms on the right side of B2 will approach zero (that is, the fast k_1 component will have reached equilibrium), and Eq. (B2) reduces to

$$\frac{\Delta_{47}^{(t)} - \Delta_{47}^{eq}}{\Delta_{47}^{init} - \Delta_{47}^{eq}} = f_2 e^{-k_2 t}. \tag{B3}$$

Taking the natural log of both sides gives

$$\ln\left[\frac{\Delta_{47}^{(t)}-\Delta_{47}^{eq}}{\Delta_{47}^{init}-\Delta_{47}^{eq}}\right] = \ln(f_2) - k_2 t. \tag{B4}$$

For convenience we term the left hand side of B4 as $\ln(1-F)$, where F is the fractional approach to equilibrium described in Appendix A. A plot of $\ln(1-F)$ versus t will have a slope equivalent to $-k_2$ and an intercept of $\ln(f_2)$. Fig. 4c and d shows such regressions for the refractory component of NE-CC-1 calcite. Criteria for selection of points to be included in such regressions are discussed below and illustrated in Fig. S2.

With values of f_2 and k_2 thus determined, the influence of the refractory pool can be subtracted from the data:

$$[1-F]' = [1-F] - f_2 e^{-k_2 t} = f_1 e^{-k_1 t}. \tag{B5}$$

In the case where values of f_2 and k_2 cannot be directly determined for the specific temperature, for example as in the 300°–425 °C data where reaction rates are too slow to clearly resolve the influence of the refractory component, the values of f_2 and k_2 are predicted using the Arrhenius parameters determined from the high temperature experiments.

A plot of $\ln[1-F]'$ versus t will have slope equivalent to $-k_1$ and intercept of $\ln(f_1)$ for each reaction temperature (Fig. 4e, f).

Fig. 4g and h shows the Arrhenius regressions for the two components identified in NE-CC-1, and Table 2 summarizes the rate constant regressions and Arrhenius parameters.

A.2. Criteria for selecting points to be included in specific temperature/ component regressions

When selecting points to be used in each straight-line regression for the long-lived component (here k_2), it is important to consider that points at early t may still reflect the contribution of the transient defect pool or the k_1 pool, and thus these points should not be included in the regression (Fig. S2a). Conversely, at very long t and high T, the Δ_{47} values may approach close to the equilibrium Δ_{47} composition, where analytical error has an increasingly large influence in the error of calculated $\ln(1-F)$ values (Fig. S2b). Thus it is important to establish a cut-off value for $\ln(1-F)$, values below which data are excluded from the regression. Selection of such a value is somewhat arbitrary, and here we use a value of -3.1, which corresponds to the approximate $\ln(1-F)$ value for a sample with $\Delta_{47} = \Delta_{47}^{equil} + 1\sigma$ (where 1σ is the analytical precision). Note that the exact $\ln(1-F)$ values for this situation vary slightly given the temperature dependence of Δ_{47}^{equil}. In addition, it is incorrect to simply establish a cut-off value on the $\ln(1-F)$ axis: doing so would bias the remaining values (included in regression) towards high values, as can be visualized in Fig. S2b (and note that such a bias already exists because $\ln(1-F)$ is undefined for Δ_{47} values that are lower than Δ_{47}^{equil}). To avoid this bias, we utilized a scheme where any value occurring later in time than the first value with $\ln(1-F) \leq -3.1$ is also excluded from the regression.

Appendix C. Error propagation for cooling rates

The equation relating cooling rate to apparent equilibrium temperature is

$$f = -dT/dt = \frac{\gamma R T_{ae}^2 k_{Tae}}{E_a} \tag{C1}$$

With the definition of each parameter given in the main text. The parameters with error are T_{ae}, k_{Tae}, and E_a, and therefore the

error equation is

$$\delta f = \sqrt{\left(\frac{\partial f}{\partial k_{Tae}}\delta k_{Tae}\right)^2 + \left(\frac{\partial f}{\partial E_a}\delta E_a\right)^2 + \left(\frac{\partial f}{\partial T_{ae}}\delta T_{ae}\right)^2} \tag{C2}$$

with the following partial derivatives:

$$\frac{\partial f}{\partial k_{Tae}} = \frac{\gamma R T_{ae}^2}{E_a} \quad \frac{\partial f}{\partial E_a} = \frac{-\gamma R T_{ae}^2 k_{Tae}}{E_a^2} \quad \frac{\partial f}{\partial T_{ae}} = \frac{2\gamma R T_{ae} k_{Tae}}{E_a}. \tag{C3}$$

The error δE_a is based on experimental data (e.g., as in Table 2), and δT_{ae} is based on the analytical uncertainty in Δ_{47} propagated through the appropriate temperature equation (for example, Eq. (5)). The rate constant k_{Tae} is given by

$$g = \ln[k_{Tae}] = \ln[k_{ref}] + \left[\frac{E_a}{R}\left(\frac{1}{T_{ref}} - \frac{1}{T_{ae}}\right)\right] \tag{C4}$$

Where the parameters with error are k_{ref}, E_a, and T_{ae}. Therefore the error equation for (C4) is

$$\delta g = \sqrt{\left(\frac{\partial g}{\partial k_{ref}}\delta k_{ref}\right)^2 + \left(\frac{\partial g}{\partial E_a}\delta E_a\right)^2 + \left(\frac{\partial g}{\partial T_c}\delta T_c\right)^2} \tag{C5}$$

with the following partial derivatives:

$$\frac{\partial g}{\partial k_{ref}} = \frac{1}{k_{ref}} \quad \frac{\partial g}{\partial E_a} = \frac{1}{R}\left[\frac{1}{T_{ref}} - \frac{1}{T_{ae}}\right] \quad \frac{\partial g}{\partial T_{ae}} = \frac{E_a}{R T_{ae}^2}. \tag{C6}$$

The errors δE_a and δT_{ae} are as described above. The reference temperature T_{ref} was taken as the inverse of the mean value of the inverse reaction temperatures used to determine rate constants. Thus for MGB-CC-1 with reaction temperatures of 658, 678, 698, 723, and 748 K, the reference temperature is

$$T_{ref} = \text{mean}(1/658, 1/678, 1/698, 1/723, 1/748)^{-1} = 699.7 \text{ K}.$$

The reference temperatures for NE-CC-1 refractory and NE-CC-1 labile are 791.6 and 745.9 K, respectively. k_{ref} values are determined by evaluating the Arrhenius regression for each material at T_{ref}, and are, for MGB-CC-1, NE-CC-1 refractory component, and NE-CC-1 labile component, respectively, 2.92×10^{-6}, 2.77×10^{-6}, and 1.42×10^{-5}. We estimate the error δk_{ref} as the mean relative error of the experimentally determined rate constants utilized in the Arrhenius regression for a particular calcite. Thus from Table 2, the mean relative errors in k values are 23%, 6.6%, and 12%, respectively, for MGB-CC-1, NE-CC-1 refractory, and NE-CC-1 labile, and the corresponding δk_{ref} values are 6.6×10^{-7}, 1.8×10^{-7}, and 1.7×10^{-6} for these respective materials. Using these values, the error in $\ln[k_{Tae}]$ is calculated using Eq. (C4). This error must then be added or subtracted from $\ln[k_{Tae}]$ *before* transforming $\ln[k_{Tae}]$ to k_{tc}. The resulting error in k_{Tae} will not be symmetric, and the unique values for the high and low errors must be propagated individually through Eq. (C2) to correctly obtain the error in cooling rate. The final errors in cooling rate are conveniently given as factors of the stated cooling rate, for example a cooling rate of 5 ($\times 6$, $\div 5$) °C/Ma corresponds to uncertainty in cooling rate ranging from 30 to 1 °C/Ma.

Appendix D. Supporting information

Supplementary data associated with this article can be found in the online version at http://dx.doi.org/10.1016/j.epsl.2012.07.021.

References

Affek, H.P., Eiler, J.M., 2006. Abundance of mass 47 CO_2 in urban air, car exhaust, and human breath. Geochim. Cosmochim. Acta 70, 1–12.

Balestrieri, M.L., Bernet, M., Brandon, M.T., Picotti, V., Reiners, P., Zattin, M., 2003. Pliocene and Pleistocene exhumation and uplift of two key areas of the Northern Apennines. Quaternary Int. 101–102, 67–73.

Bristow, T.F., Bonifacie, M., Derkowski, A., Eiler, J.M., Grotzinger, J.P., 2011. A hydrothermal origin for isotopically anomalous cap dolostone cements from south China. Nature 474, 68–71.

Came, R.E., Eiler, J.M., Veizer, J., Azmy, K., Brand, U., Weidman, C.R., 2007. Coupling of surface temperatures and atmospheric CO_2 concentrations during the Paleozoic era. Nature 449, 198–201.

Carmignani, L., Kligfield, R., 1990. Crustal extension in the Northern Apennines: the transition from compression to extension in the Alpi Apuane core complex. Tectonics 9, 1275–1303.

Cerling, T.E., Ayliffe, L.K., Dearing, M.D., Ehleringer, J.R., Passey, B.H., Podlesak, D.W., Torregrossa, A.-M., West, A.G., 2007. Determining biological tissue turnover using stable isotopes: the reaction progress variable. Oecologia 151, 175–189.

Dennis, K.J., Schrag, D.P., 2010. Clumped isotope thermometry of carbonatites as an indicator of diagenetic alteration. Geochim. Cosmochim. Acta 74, 4110–4122.

Dennis, K.J., Affek, H.P., Passey, B.H., Schrag, D.P., Eiler, J.M., 2011. Defining an absolute reference frame for 'clumped' isotope studies of CO_2. Geochim. Cosmochim. Acta 75, 7117–7131.

Dodson, M.H., 1973. Closure temperature in cooling geochronological and petrological systems. Contrib. Mineral. Petrol. 40, 259–274.

Farver, J.R., 1994. Oxygen self-diffusion in calcite: dependence on temperature and water fugacity. Earth Planet. Sci. Lett. 121, 575–587.

Fellin, M.G., Reiners, P.W., Brandon, M.T., Wüthrich, E., Balestrieri, M.L., Molli, G., 2007. Thermochronologic evidence for the exhumational history of the Alpi Apuane metamorphic core complex, northern Apennines, Italy. Tectonics 26 (TC6015), 1–22.

Ferry, J.M., Passey, B.H., Vasconcelos, C., Eiler, J.M., 2011. Formation of dolomite at 40–80C in the Latemar carbonate buildup, Dolomites, Italy, from clumped isotope thermometry. Geology 39, 571–574.

Finnegan, S., Bergmann, K., Eiler, J.M., Jones, D.S., Fike, D.A., Eisenman, I., Hughes, N.C., Tripati, A.K., Fischer, W.W., 2011. The magnitude and duration of late Ordovician–early Silurian glaciation. Science 331, 903–906.

Friedlander, G., Kennedy, J.W., Macias, E.S., Miller, J.M., 1981. Nuclear and Radiochemistry. Wiley, New York 684 pp.

Ghosh, P., Adkins, J., Affek, H., Balta, B., Guo, W., Schauble, E.A., Schrag, D., Eiler, J.M., 2006. ^{13}C–^{18}O bonds in carbonate minerals: a new kind of paleothermometer. Geochim. Cosmochim. Acta 70, 1439–1456.

Guo, W., Mosenfelder, J.L., Goddard, W.A., Eiler, J.M., 2009. Isotopic fractionations associated with phosphoric acid digestion of carbonate minerals: insights from first-principles theoretical modeling and clumped isotope measurements. Geochim. Cosmochim. Acta 73, 7203–7225.

Herz, N., Dean, N.E., 1986. Stable isotopes and archaeological geology: the Carrara marble, northern Italy. Appl. Geochem. 1, 139–151.

Huntington, K.W., Eiler, J.M., Affek, H.P., Guo, W., Bonifacie, M., Yeung, L.Y., Thiagarajan, N., Passey, B., Tripati, A., Daëron, M., Came, R., 2009. Methods and limitations of 'clumped' CO_2 isotope ($D47$) analysis by gas-source isotope ratio mass spectrometry. J. Mass Spectrom. 44, 1318–1329.

Huntington, K.W., Budd, D.A., Wernicke, B.P., Eiler, J.M., 2011. Use of clumped-isotope thermometry to constrain the crystallization temperature of diagenetic calcite. J. Sediment. Res. 81, 656–669.

Keating-Bitonti, C.R., Ivany, L.C., Affek, H.P., Douglas, P., Samson, S.D., 2011. Warm, not super-hot, temperatures in the early Eocene subtropics. Geology 39, 771–774.

Kligfield, R., Hunziker, J., Dallmeyer, R.D., Schamel, S., 1986. Dating of deformation phases using K–Ar and ^{40}Ar/^{39}Ar techniques: results from the Northern Apennines. J. Struct. Geol. 8, 781–798.

Kronenberg, A.K., Yund, R.A., Giletti, B.J., 1984. Carbon and oxygen diffusion in calcite: effects of Mn content and P_{H2O}. Phys. Chem. Miner. 11, 101–112.

Labotka, T.C., Cole, D.R., Riciputi, L.R., Fayek, M., 2004. Diffusion of C and O in calcite from 0.1 to 200 MPa. Am. Mineral. 89, 799–806.

Labotka, T.C., Cole, D.R., Fayek, M.T., Chacko, T., 2011. An experimental study of the diffusion of C and O in calcite in mixed CO_2–H_2O fluids. Am. Mineral. 96, 1262–1269.

Passey, B.H., Levin, N.E., Cerling, T.E., Brown, F.H., Eiler, J.M., 2010. High-temperature environments of human evolution in East Africa based on bond ordering in paleosol carbonates. Proc. Natl. Acad. Sci. USA 107, 11245–11249.

Preston-Thomas, H., 1990. The international temperature scale of 1990 (ITS-90). Metrologia 27, 3–10.

Reiners, P.W., Ehlers, T.A., Zeitler, P.K., 2005. Past, present, and future of thermochronology. Rev. Mineral. Geochem. 58, 1–18.

Schauble, E.A., Ghosh, P., Eiler, J.M., 2006. Preferential formation of ^{13}C–^{18}O bonds in carbonate minerals, estimated using first-principles lattice dynamics. Geochim. Cosmochim. Acta 70, 2510–2529.

Schmid, T., Bernasconni, S., 2010. An automated method for "clumped-isotope" measurements on small carbonate samples. Rapid Commun. Mass Spectrom. 24, 1955–1963.

Wang, Z., Schauble, E.A., Eiler, J.M., 2004. Equilibrium thermodynamics of multiply substituted isotopologues and molecular gases. Geochim. Cosmochim. Acta 68, 4779–4797.

Zhang, Y., 1994. Reaction kinetics, geospeedometry, and relaxation theory. Earth Planet. Sci. Lett. 122, 373–391.

Zhang, Y., 2008. Geochemical Kinetics. Princeton University Press, Princeton 631 pp.
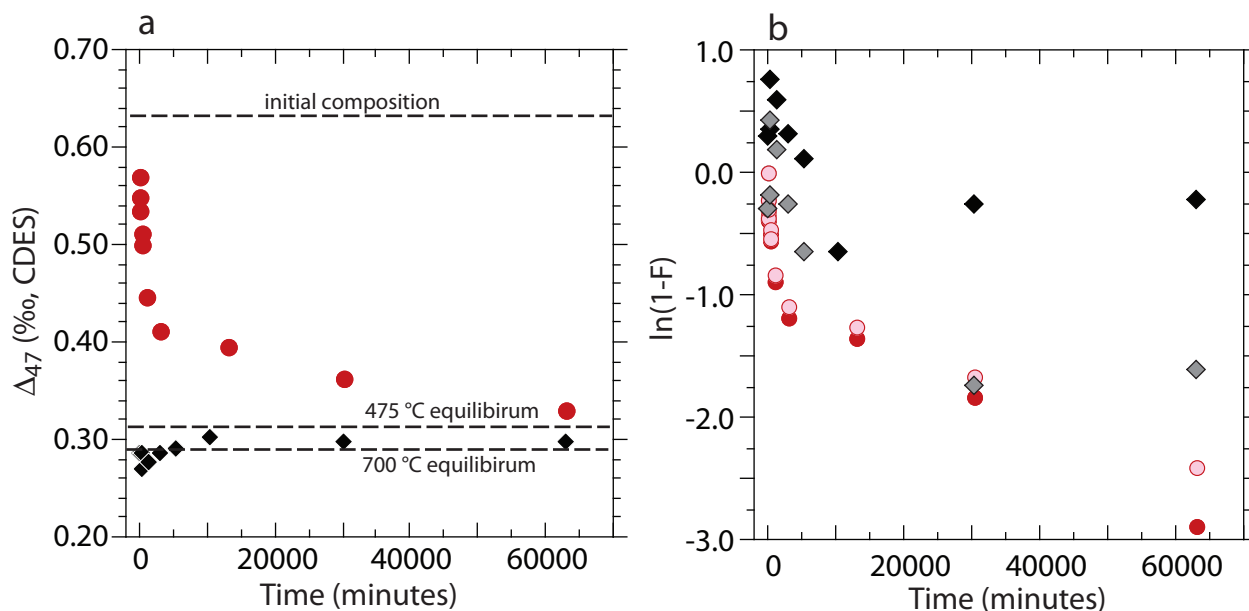
Fig. S1. Comparison of order-disorder experiments (red circles) with disorder-order experiments (black diamonds) conducted at 475 °C on NE-CC-1 calcite. a) The equilibrium compositions predicted by Eq. 5 are shown as dashed lines. b) The same data plotted as first-order reaction progress. The gray diamonds and pink circles are the same data, but with reaction progress recalculated using equilibrium Δ47 values predicted from Eq. 4 instead of Eq. 5 (that is, equilibrium values that are not shifted by +0.012 per mil, as described in Methods). Note that use of Eq. 4 versus Eq. 5 has little effect on calculated reaction progress for order-disorder reactions (red / pink circles), whereas it has a large effect for disorder-order reactions (black / gray diamonds). This is because the Δ47 values of the latter are always within a few hundredths of per mil of the equilibrium value, so the shift in equilibrium values of 0.012 per mil has a relatively large impact on the calculation of (1-F).
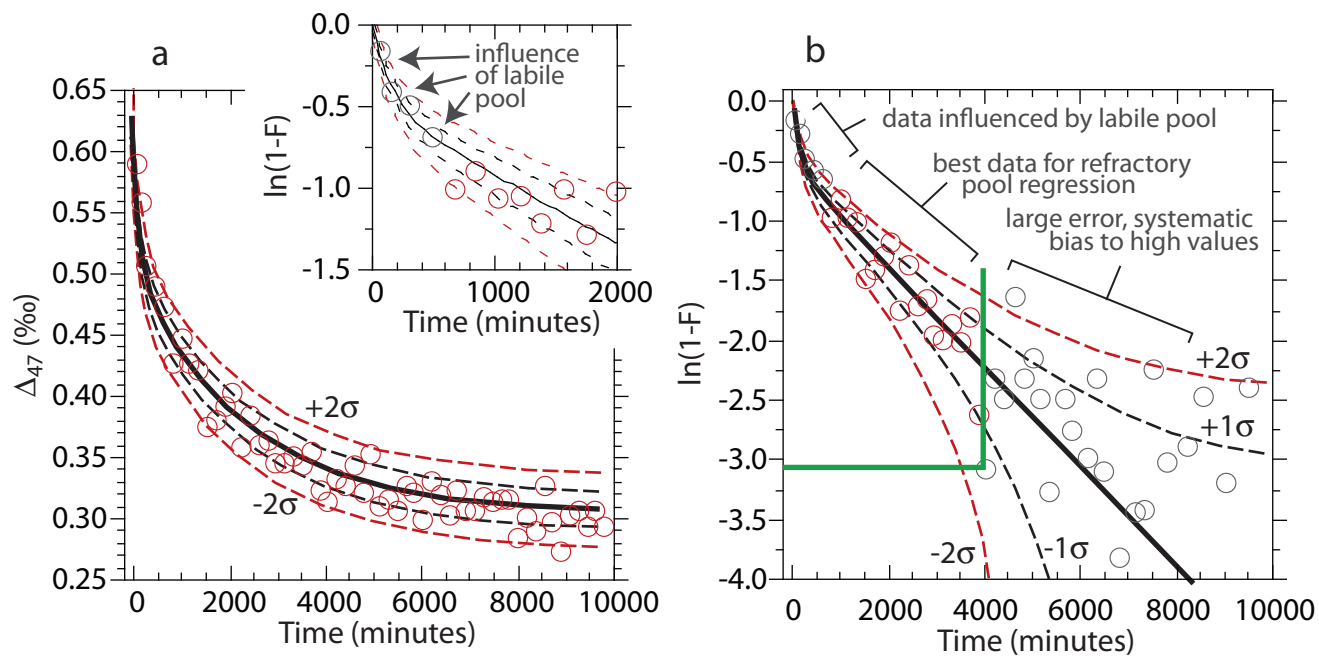
Fig. S2. Illustration of the influence of analytical error on rate constant regressions, and of the scheme used as a 'cut off' for data points approaching close to equilibrium. a) Reaction progress of a hypothetical two-component mechanical mixture system. Red circles are synthetic data with randomly generated error equivalent to the analytical precision for Δ47 of 0.013‰. b) The same data plotted as ln(1-F). Red circles are data points that would be included in the regression identifying the rate constant of the refractory pool. Green lines show the 'cut off' values, as explained in Appendix B.

Table S1. Results for MGB-CC-1 calcite heating experiments conducted under dry conditions

Reaction ID	T (°C)	Time (minutes)	$\delta^{13}C$ (PDB)	$\delta^{18}O$ (PDB)	Δ_{47} (Ghosh)*	Δ_{47} (CDES)†
unreacted (n = 3)		-	-4.81	-9.35	0.581	0.634
		± 1σ	±0.01	±0.05	±0.014	±0.008
RDX187	385	31	-4.81	-9.35	0.557	0.612
RDX185	385	61	-4.82	-9.37	0.550	0.605
RDX183	385	121	-4.80	-9.36	0.526	0.580
RDX182	385	242	-4.81	-9.38	0.537	0.591
RDX189	385	944	-4.82	-9.30	0.506	0.558
RDX181	385	2729	-4.83	-9.37	0.498	0.550
RDX176	405	30	-4.84	-9.43	0.550	0.605
RDX176	405	30	-4.80	-9.35	0.555	0.610
RDX179	405	61	-4.79	-9.35	0.524	0.577
RDX179	405	61	-4.82	-9.37	0.545	0.599
RDX178	405	90	-4.80	-9.38	0.518	0.571
RDX178	405	90	-4.84	-9.37	0.508	0.560
RDX171	405	124	-4.81	-9.41	0.530	0.583
RDX171	405	124	-4.83	-9.40	0.494	0.545
RDX168	405	239	-4.83	-9.35	0.529	0.583
RDX168	405	239	-4.81	-9.34	0.513	0.566
RDX175	405	449	-4.82	-9.39	0.507	0.537
RDX175	405	449	-4.81	-9.38	0.481	0.553
RDX169	405	1349	-4.83	-9.36	0.464	0.513
RDX169	405	1349	-4.82	-9.35	0.476	0.526
RDX173	405	2827	-4.81	-9.40	0.445	0.493
RDX173	405	2827	-4.83	-9.36	0.470	0.520
RDX177	405	8608	-4.82	-9.38	0.387	0.432
RDX172	425	30	-4.84	-9.39	0.508	0.560
RDX172	425	30	-4.83	-9.36	0.522	0.575
RDX167	425	50	-4.80	-9.43	0.498	0.550
RDX167	425	50	-4.83	-9.34	0.487	0.538
RDX170	425	70	-4.76	-9.35	0.485	0.536
RDX170	425	70	-4.82	-9.37	0.515	0.587
RDX166	425	90	-4.82	-9.42	0.490	0.541
RDX166	425	90	-4.81	-9.43	0.494	0.550
RDX174	425	110	-4.84	-9.45	0.486	0.537
RDX174	425	110	-4.82	-9.39	0.502	0.553
RDX152	425	120	-4.83	-9.39	0.465	0.517
RDX152	425	120	-4.83	-9.38	0.463	0.514
RDX154	425	240	-4.83	-9.40	0.452	0.503
RDX154	425	240	-4.81	-9.55	0.473	0.525

Table S1. Results for MGB-CC-1 calcite heating experiments conducted under dry conditions

Reaction ID	T (°C)	Time (minutes)	$\delta^{13}C$ (PDB)	$\delta^{18}O$ (PDB)	Δ_{47} (Ghosh)*	Δ_{47} (CDES)†
RDX150	425	480	-4.82	-9.42	0.439	0.490
RDX150	425	480	-4.82	-9.43	0.437	0.487
RDX151	425	1380	-4.72	-9.50	0.417	0.466
RDX149	425	2880	-4.83	-9.42	0.398	0.445
RDX149	425	2880	-4.81	-9.43	0.386	0.432
RDX153	425	5840	-4.83	-9.43	0.363	0.409
RDX153	425	5840	-4.84	-9.40	0.364	0.409
RDX143	450	121	-4.83	-9.41	0.430	0.475
RDX146	450	260	-4.81	-9.35	0.400	0.443
RDX148	450	425	-4.83	-9.38	0.385	0.428
RDX147	450	600	-4.81	-9.38	0.362	0.404
RDX145	450	1440	-4.81	-9.40	0.352	0.393
RDX144	450	2880	-4.84	-9.36	0.307	0.346
RDX112	475	121	-4.83	-9.34	0.382	0.422
RDX113	475	253	-4.83	-9.30	0.371	0.411
RDX114	475	479	-4.82	-9.39	0.340	0.378
RDX115	475	1017	-4.82	-9.32	0.297	0.333
RDX116	475	2939	-4.81	-9.31	0.284	0.320
RDX117	475	5986	-4.82	-9.33	0.296	0.332
RDX121§	475	631	-4.81	-9.33	0.308	0.345
RDX120§	475	5757	-4.83	-9.29	0.285	0.320

Note: Analytical precision for Δ_{47} is 0.013‰ (1σ). Analytical precision for $\delta^{13}C$, $\delta^{18}O$ is better than 0.1‰.

* Δ_{47} values relative to the 'heated gas scale' (Ghosh et al., 2006; Huntington et al., 2009).

† Δ_{47} values relative to the 'carbon dioxide equilibrium scale' (CDES) described by Dennis et al., 2011.

§ ~10 mg of water was intentionally added to reaction tubes to evaluate the effect of water on reordering rates

Table S2. Results for NE-CC-1 calcite heating experiments conducted under dry conditions.

Reaction ID	T (°C)	Time (min)	$\delta^{13}C$ (PDB)	$\delta^{18}O$ (PDB)	Δ_{47} (Ghosh)[a]	Δ_{47} (CDES)[b]
NE-CC-1 60-120 mesh (spar calcite)						
unreacted (n = 7)			6.73	-15.88	0.583	0.636
(1σ)		-	±0.02	±0.05	±0.015	±0.015
RDX020	100	30	-6.70	-15.85	0.564	0.621
RDX090	130	5678	-6.71	-15.88	0.597	0.651
RDX100	300	66	-6.78	-15.95	0.596	0.642
RDX100	300	66	-6.75	-15.86	0.590	0.638
RDX104	300	219	-6.73	-15.93	0.584	0.631
RDX104	300	219	-6.67	-15.81	0.571	0.619
RDX105	300	300	-6.74	-15.98	0.556	0.601
RDX105	300	300	-6.70	-15.77	0.549	0.596
RDX102	300	492	-6.73	-15.90	0.573	0.620
RDX102	300	492	-6.67	-15.79	0.563	0.611
RDX101	300	933	-6.76	-15.97	0.565	0.610
RDX058	300	1483	-6.79	-15.95	0.572	0.625
RDX110	300	1821	-6.71	-15.86	0.572	0.618
RDX059	300	5553	-6.74	-15.90	0.562	0.614
RDX109	350	57	-6.75	-15.95	0.570	0.615
RDX109	350	57	-6.75	-15.88	0.567	0.615
RDX108	350	216	-6.66	-15.70	0.543	0.587
RDX108	350	216	-6.74	-15.93	0.563	0.613
RDX099	350	296	-6.73	-15.99	0.576	0.621
RDX099	350	296	-6.70	-15.79	0.552	0.599
RDX107	350	483	-6.72	-15.81	0.556	0.600
RDX107	350	483	-6.73	-15.86	0.553	0.600
RDX106	350	1370	-6.77	-15.98	0.563	0.608
RDX103	350	5445	-6.76	-15.88	0.550	0.593
RDX129	385	30	-6.75	-15.95	0.568	0.618
RDX122	385	90	-6.77	-15.98	0.566	0.616
RDX127	385	150	-6.77	-15.99	0.575	0.626
RDX124	385	300	-6.78	-16.05	0.575	0.625
RDX128	385	646	-6.77	-15.96	0.542	0.590
RDX092	425	30	-6.77	-15.93	0.567	0.619
RDX094	425	60	-6.74	-15.97	0.554	0.605
RDX095	425	90	-6.76	-15.91	0.529	0.580
RDX091	425	120	-6.76	-15.95	0.538	0.589
RDX093	425	153	-6.70	-15.84	0.527	0.578
RDX065	425	116	-6.72	-15.82	0.519	0.555
RDX060	425	316	-6.68	-15.74	0.510	0.546
RDX064	425	606	-6.74	-15.87	0.508	0.545
RDX061	425	1454	-6.67	-15.83	0.491	0.536
RDX063	425	4598	-6.74	-15.87	0.441	0.484

Table S2. Results for NE-CC-1 calcite heating experiments conducted under dry conditions.

Reaction ID	T (°C)	Time (min)	$\delta^{13}C$ (PDB)	$\delta^{18}O$ (PDB)	Δ_{47} (Ghosh)[a]	Δ_{47} (CDES)[b]
RDX062	425	14452	-6.74	-15.87	0.397	0.431
RDX062	425	14452	-6.75	-15.84	0.427	0.468
RDX126	475	32	-6.73	-15.99	0.523	0.570
RDX125	475	59	-6.75	-16.03	0.490	0.536
RDX123	475	89	-6.75	-16.01	0.487	0.534
RDX130	475	120	-6.74	-15.95	0.488	0.535
RDX022	475	120	-6.73	-15.86	0.507	0.562
RDX023	475	240	-6.71	-15.83	0.459	0.511
RDX027	475	450	-6.75	-15.93	0.448	0.499
RDX024	475	1080	-6.76	-15.90	0.400	0.447
RDX025	475	2880	-6.70	-15.88	0.367	0.412
RDX016	475	12960	-6.74	-15.89	0.351	0.396
RDX042	475	30214	-6.74	-15.77	0.320	0.359
RDX042	475	30214	-6.78	-15.80	0.330	0.369
RDX046	475	62924	-6.73	-15.85	0.299	0.331
RDX026	525	60	-6.68	-15.84	0.411	0.459
RDX019	525	180	-6.73	-15.89	0.371	0.417
RDX021	525	358	-6.71	-15.83	0.330	0.373
RDX010	525	718	-6.64	-15.74	0.332	0.375
RDX017	525	1438	-6.74	-15.90	0.320	0.362
RDX018	525	2878	-6.72	-15.80	0.305	0.346
RDX015	525	5766	-6.72	-15.82	0.287	0.328
RDX038	560	30	-6.67	-15.86	0.365	0.410
RDX031	560	58	-6.72	-15.90	0.356	0.401
RDX037	560	186	-6.66	-15.82	0.319	0.361
RDX036	560	428	-6.70	-15.83	0.308	0.350
RDX034	560	1262	-6.72	-15.88	0.288	0.328
RDX045	560	5416	-6.72	-15.80	0.281	0.319
RDX048	560	30199	-6.78	-15.84	0.265	0.302
RDX048	560	30199	-6.80	-15.94	0.259	0.294
RDX047	560	41689	-6.75	-15.79	0.273	0.309
RDX002	600	58	-6.77	-15.97	0.296	0.336
RDX004	600	180	-6.75	-15.87	0.273	0.312
RDX007	600	359	-6.63	-15.75	0.266	0.304
RDX009	600	1080	-6.71	-15.88	0.263	0.301
RDX005	600	2160	-6.75	-15.91	0.261	0.300
RDX013	650	30	-6.72	-15.87	0.269	0.308
RDX006	650	60	-6.63	-15.71	0.282	0.322
RDX012	650	180	-6.73	-15.86	0.258	0.297
RDX001	650	360	-6.66	-15.76	0.249	0.287

Table S2. Results for NE-CC-1 calcite heating experiments conducted under dry conditions.

Reaction ID	T (°C)	Time (min)	$\delta^{13}C$ (PDB)	$\delta^{18}O$ (PDB)	Δ_{47} (Ghosh)[a]	Δ_{47} (CDES)[b]
RDX003	650	1440	-6.76	-15.89	0.238	0.275
RDX011	650	2890	-6.72	-15.85	0.246	0.284
RDX008	650	5761	-6.56	-15.58	0.247	0.284
RDX030	700	1208	-6.77	-15.93	0.251	0.289
RDX030	700	1208	-6.80	-15.93	0.255	0.290
RDX057	800	199	-6.81	-15.99	0.259	0.294
RDX056	800	2158	-6.85	-16.14	0.259	0.294
NE-CC-1 120-270 mesh[c]						
RDX096	425	152	-6.73	-15.92	0.533	0.584
NE-CC-1 single ~15mg grain[c]						
RDX098	425	154	-7.57	-17.05	0.571	0.624
NE-CC-1 60-120 mesh[c]						
RDX088	425	150	-6.71	-15.94	0.526	0.576
NE-CC-1 60-120 mesh, preannealed[d]						
RDX032	475	120	-6.74	-15.92	0.254	0.292
RDX032	475	120	-6.79	-15.98	0.245	0.280
RDX035	475	238	-6.77	-15.94	0.233	0.269
RDX035	475	238	-6.80	-15.95	0.238	0.272
RDX029	475	481	-6.77	-15.97	0.245	0.282
RDX029	475	481	-6.81	-16.01	0.252	0.287
RDX028	475	1270	-6.74	-15.89	0.235	0.272
RDX028	475	1270	-6.73	-15.98	0.247	0.282
RDX033	475	2885	-6.78	-16.00	0.251	0.289
RDX033	475	2885	-6.76	-15.89	0.247	0.282
RDX049	475	5436	-6.81	-15.84	0.270	0.306
RDX049	475	5436	-6.82	-15.98	0.241	0.275
RDX039	475	10415	-6.81	-15.91	0.279	0.316
RDX039	475	10415	-6.80	-16.01	0.254	0.289
RDX040	475	30215	-6.76	-15.85	0.257	0.293
RDX040	475	30215	-6.73	-15.85	0.266	0.302
RDX043	475	62920	-6.79	-16.01	0.262	0.297

a. Δ_{47} values reported on the heated gas scale sensu Ghosh et al., 2006; Huntington et al., 2009.
b. Δ_{47} values reported on the 'carbon dioxide equilibrium scale' described by Dennis et al., 2011.
c. Samples subjected to oven drying at 130 °C for 5678 min. prior to reaction.
d. Samples preannealed at 700 °C for 1208 min. prior to reaction. These are 'disorder-order' direction experiments.

Table S3. Results for NE-CC-1 calcite heating experiments conducted in water at high pressure.

Reaction ID	Mesh Size	T (°C)	Time (min)	Pressure (MPa)	Reaction Capsule	$\delta^{13}C$ (PDB)	$\delta^{18}O$ (PDB)	Δ_{47} (Ghosh)[a]	Δ_{47} (CDES)[b]
RDX157	60-120[c]	-	-	-	silver	-6.77	-15.84	0.605	0.666
RDX158	60-120[c]	-	-	-	silver	-6.75	-15.88	0.552	0.610
RDX159	60-120[c]	-	-	-	gold	-6.73	-15.89	0.580	0.640
RDX160	60-120	422	124	100	gold	-6.75	-15.95	0.549	0.606
RDX162	120-270	422	124	100	silver	-6.75	-15.99	0.523	0.579
RDX161	60-120	422	125	100	silver	-6.73	-15.94	0.529	0.586
RDX155	60-120	422	307	100	silver	-6.76	-15.96	0.500	0.555
RDX156	60-120	422	307	100	gold	-6.77	-16.06	0.528	0.585
RDX163	60-120	420	621	50-100[d]	gold	-6.71	-16.03	0.494	0.547
RDX165	120-270	421	4298	100	silver	-6.75	-16.11	0.433	0.482
RDX164	60-120	421	4292	100	silver	-6.76	-16.13	0.394	0.441

a. Δ_{47} values reported on the heated gas scale sensu Ghosh et al., 2006; Huntington et al., 2009.
b. Δ_{47} values reported on the 'carbon dioxide equilibrium scale' described by Dennis et al., 2011.
c. These samples were not subjected to high temperature annealing. They serve to evaluate the effect of the capsule welding process on clumped isotope compositions. The RDX158 capsule ruptured during welding due to overheating. All other capsules were wrapped in wet tissue during welding in an effort to buffer temperatures near 100 °C.
d. Reaction vessel was not leak-tight; pressure cycled between ~50 and 100 MPa during course of reaction.